NASA/TM—2013-217868

# Effects of Microstructural Parameters on Creep of Nickel-Base Superalloy Single Crystals

*Rebecca A. MacKay, Timothy P. Gabb, and Michael V. Nathal*
*Glenn Research Center, Cleveland, Ohio*

April 2013

# NASA STI Program . . . in Profile

Since its founding, NASA has been dedicated to the advancement of aeronautics and space science. The NASA Scientific and Technical Information (STI) program plays a key part in helping NASA maintain this important role.

The NASA STI Program operates under the auspices of the Agency Chief Information Officer. It collects, organizes, provides for archiving, and disseminates NASA's STI. The NASA STI program provides access to the NASA Aeronautics and Space Database and its public interface, the NASA Technical Reports Server, thus providing one of the largest collections of aeronautical and space science STI in the world. Results are published in both non-NASA channels and by NASA in the NASA STI Report Series, which includes the following report types:

- TECHNICAL PUBLICATION. Reports of completed research or a major significant phase of research that present the results of NASA programs and include extensive data or theoretical analysis. Includes compilations of significant scientific and technical data and information deemed to be of continuing reference value. NASA counterpart of peer-reviewed formal professional papers but has less stringent limitations on manuscript length and extent of graphic presentations.

- TECHNICAL MEMORANDUM. Scientific and technical findings that are preliminary or of specialized interest, e.g., quick release reports, working papers, and bibliographies that contain minimal annotation. Does not contain extensive analysis.

- CONTRACTOR REPORT. Scientific and technical findings by NASA-sponsored contractors and grantees.

- CONFERENCE PUBLICATION. Collected papers from scientific and technical conferences, symposia, seminars, or other meetings sponsored or cosponsored by NASA.

- SPECIAL PUBLICATION. Scientific, technical, or historical information from NASA programs, projects, and missions, often concerned with subjects having substantial public interest.

- TECHNICAL TRANSLATION. English-language translations of foreign scientific and technical material pertinent to NASA's mission.

Specialized services also include creating custom thesauri, building customized databases, organizing and publishing research results.

For more information about the NASA STI program, see the following:

- Access the NASA STI program home page at *http://www.sti.nasa.gov*

- E-mail your question to *help@sti.nasa.gov*

- Fax your question to the NASA STI Information Desk at 443–757–5803

- Phone the NASA STI Information Desk at 443–757–5802

- Write to:
  STI Information Desk
  NASA Center for AeroSpace Information
  7115 Standard Drive
  Hanover, MD 21076–1320

NASA/TM—2013-217868

# Effects of Microstructural Parameters on Creep of Nickel-Base Superalloy Single Crystals

*Rebecca A. MacKay, Timothy P. Gabb, and Michael V. Nathal*
*Glenn Research Center, Cleveland, Ohio*

National Aeronautics and
Space Administration

Glenn Research Center
Cleveland, Ohio 44135

April 2013

## Acknowledgments

The authors wish to acknowledge Dr. Anita Garg of University of Toledo for performing scanning electron microscopy on the $\gamma$–$\gamma'$ microstructures. This work was supported by the Subsonic Fixed Wing project under the Fundamental Aeronautics Program at the NASA Glenn Research Center.



This work was sponsored by the Fundamental Aeronautics Program at the NASA Glenn Research Center.

*Level of Review*: This material has been technically reviewed by technical management.

Available from

NASA Center for Aerospace Information
7115 Standard Drive
Hanover, MD 21076–1320

National Technical Information Service
5301 Shawnee Road
Alexandria, VA 22312

Available electronically at http://www.sti.nasa.gov

# Effects of Microstructural Parameters on Creep of Nickel-Base Superalloy Single Crystals

Rebecca A. MacKay, Timothy P. Gabb, and Michael V. Nathal
National Aeronautics and Space Administration
Glenn Research Center
Cleveland, Ohio 44315

## Abstract

Microstructure-sensitive creep models have been developed for Ni-base superalloy single crystals. Creep rupture testing was conducted on fourteen single crystal alloys at two applied stress levels at each of two temperatures, 982 and 1093 °C. The variation in creep lives among the different alloys could be explained with regression models containing relatively few microstructural parameters. At 982 °C, g - g¢ lattice mismatch, g¢ volume fraction, and initial g¢ size were statistically significant in explaining the creep rupture lives. At 1093 °C, only lattice mismatch and g¢ volume fraction were significant. These models could explain from 84 to 94 percent of the variation in creep lives, depending on test condition. Longer creep lives were associated with alloys having more negative lattice mismatch, lower g¢ volume fractions, and finer g¢ sizes. The g - g¢ lattice mismatch exhibited the strongest influence of all the microstructural parameters at both temperatures. Although a majority of the alloys in this study were stable with respect to topologically close packed (TCP) phases, it appeared that up to ~2 vol% TCP phase did not affect the 1093 °C creep lives under applied stresses that produced lives of ~200 to 300 h. In contrast, TCP phase contents of ~2 vol% were detrimental at lower applied stresses where creep lives were longer. A regression model was also developed for the as-heat treated initial g¢ size; this model showed that g¢ solvus temperature, g - g¢ lattice mismatch, and bulk Re content were all statistically significant.

## Introduction

Single crystal superalloys are used in turbine blade applications where high temperature creep resistance is required. Creep of superalloy single crystals can be generalized to fall into three temperature/stress regimes (Refs. 1 to 3). The low temperature regime (~750 °C) is characterized by stable g¢ microstructures, and deformation proceeds by g¢ shearing at high stresses and bypassing at lower stresses. The intermediate temperature regime (~850 to 1000 °C) is sometimes termed the 'tertiary creep' regime (Refs. 2, 4, and 5). Here, the creep curve does not exhibit a true steady state region, but instead shows a continuously increasing creep rate from a minimum strain rate until failure occurs. In this regime, particle bypassing is again expected to dominate, and a gradual directional coarsening of the g¢ phase (i.e., g¢ rafting) is one of several softening mechanisms responsible for tertiary creep. At high temperatures (~1000 to 1150 °C), rafting is very rapid and more frequently regarded as a strengthening effect. However, the actual transitions between the three creep temperature regimes are highly alloy dependent. For example, first generation superalloys with 0 wt% Re can exhibit rapid rafting at temperatures as low as 980 to 1000 °C, whereas the 3 wt% Re addition in second generation alloys tends to push the rafting regime to at least 1050 °C. Since increasing the temperature capability of turbine blades for future engines drives new alloy development, high temperature creep between 980 and 1100 °C will be emphasized in this paper.

The influences of numerous microstructural features, as well as composition, on the creep properties of Ni-base superalloy single crystals have been studied for many years, and a summary of observed effects is given below. A key microstructural parameter affecting creep is the g¢ volume fraction (Refs. 6 to 9), which must be high enough to restrict dislocation motion in the g matrix channels between neighboring g¢ precipitates (Ref. 1). Empirical results on single crystals of alloy TMS-75 (Ref. 8) showed

a strong peak in rupture life as a function of g¢ volume fraction. This work concluded that the optimized g¢ volume fraction in this alloy was ~70 vol% for maximum creep life at 900 °C and ~55 vol% for maximum life at 1100 °C. Increases in the g¢ volume fraction were also believed to be partially responsible for improved creep resistance of other first-generation single crystals at 1000 °C (Ref. 7). Another study indicated that improved creep lives were exhibited at 1150 °C when higher g¢ volume fractions were present in alloys as a result of their increased g¢ solvus temperatures (Ref. 10). However at lower temperatures of 980 to 1050 °C, this beneficial effect of higher g¢ solvus temperature was not apparent. Instead, longer lives at 980 °C were primarily attributed to solid solution hardening by Re additions, whereas longer lives at 1050 °C were associated with faster g¢ rafting kinetics and a more stable rafted structure (Ref. 10). Other work concluded that alloys should not be designed to maximize the g¢ volume fraction at creep temperatures between 1000 and 1100 °C (Ref. 9) because microstructural changes were correlated with an early onset of third-stage creep when the g¢ volume fractions exceeded 50 vol% at these elevated temperatures.

The lattice mismatch between the g and g¢ phases has also received much attention as a vital factor affecting creep resistance (Refs. 6, 7, 10 to 17), and an optimum mismatch value is dependent upon the operative creep regime. Several papers showed increased creep lives with more negative values of lattice mismatch (Refs. 7, 11, 16, 18, and 19). Experimental studies demonstrated that increasing the magnitude of lattice mismatch increased g¢ rafting kinetics (Refs. 14, 16, and 20) and decreased the spacing of misfit dislocation networks that developed at the g - g¢ interfaces (Refs. 12, 16, 19, and 21). Finer dislocation network spacings have been correlated with improved creep lives and minimum creep rates (Refs. 7, 12, 16, 19, and 22). In contrast, Caron (Ref. 10) observed no clear relationship between calculated values of lattice mismatch and creep resistance at and above 950 °C.

A number of studies (Refs. 11, 12, 23 to 25) demonstrated a relationship between the initial g¢ particle size and creep properties near 1000 °C. Early studies (Refs. 11, 12, 23, and 24) showed that the initial g¢ size and distribution influenced subsequent raft formation and perfection. The optimum initial microstructure for high temperature creep resistance was characterized by cuboidal g¢ precipitates that were strongly aligned along {001} directions in the microstructure; some alloys achieved this optimum microstructure with a refinement in the g¢ size (Ref. 24), whereas other alloys attained this with coarser g¢ particles (Ref. 23). Nathal (Ref. 12) showed that the influence of initial g¢ size was most prominent in alloys with large negative values of lattice mismatch, which appeared to be related to the influence of mismatch on the g¢ morphology at a given particle size. This is consistent with more recent work (Ref. 25) on Re and Ru-bearing alloys. Creep resistance was correlated with the number of lamellar g - g¢ interfaces in the rafted structure and with linear termination densities (Ref. 12), suggesting that irregularities in the lamellar structure were weakening microstructural features.

The precipitation of topologically closed packed (TCP) phases is another microstructural parameter affected by alloying. As a material becomes more saturated with refractory metals, solid solution strengthening increases creep resistance. However when an alloy becomes oversaturated with a refractory element, detrimental quantities of TCP phases can form. The TCP phases are believed to decrease creep properties by depleting the amount of refractory elements in solution in the g matrix (Refs. 13 and 26), or by inducing localized deformation in single crystals through creep cavitation (Refs. 4 and 27). TCP phase precipitation can also cause discontinuities with the regular g¢ rafted structure (Refs. 13, 26 to 28), which provide paths for mobile dislocations to circumvent the interfacial barriers.

Thus, it is apparent that numerous microstructural parameters have been shown to affect creep properties, although the relative influence of each is unclear and opposing trends are sometimes observed between different studies. The influence of alloying elements on creep properties is also not entirely understood although progress has been made (Ref. 29). The effect of an element is dependent upon the presence or absence of other elements in the alloy, and an individual element can influence strengthening mechanisms by simultaneously affecting a number of the microstructural factors.

The purpose of the present paper is to provide further insight on the relative influence of the microstructural parameters that control creep resistance in single crystal superalloys in the high temperature creep regime between 980 and 1100 °C. A new series of alloys, termed Low Density Single Crystals (LDS), has been developed for potential turbine blade applications (Refs. 30 to 32) and was studied in this paper. The LDS alloys contain fixed contents of Al and Ta for g¢precipitation and variations in the levels of Cr, Co, Mo, and Re. We have previously developed statistical regression models to determine the effect of composition on key microstructural parameters in this LDS alloy series (Refs. 33 and 34). Specifically, g¢solvus, g¢volume fraction, TCP phase volume fraction, g and g¢phase chemistries, and g - g¢lattice mismatch were explored in detail. Quantitative assessments of these microstructural parameters from our previous work will be presented herein only in summary form. It is expected that the creep models developed in the present study, coupled with the composition-dependent microstructural parameter models developed earlier, will enhance future alloy optimization.

## Materials and Experimental Procedures

Fourteen LDS alloys were cast into single crystal slabs at a commercial casting vendor, PCC Airfoils LLC, Minerva, Ohio. A design of experiments (DOE) approach (Refs. 31 and 32) was employed that minimized the number of alloys that was necessary to be cast. The aim baseline alloy selected for this design strategy contained 6.1 wt% Al, 6.2 wt% Ta, 50 to 100 ppm wt% Y, and a balance of Ni. Alloying elements were varied as follows: 0 to 5 wt% Cr; 0 to 11 wt% Co; 6 to 12 wt% Mo; and 0 to 4 wt% Re. The DOE and selected element ranges (Refs. 31 and 32) enabled good predictive capabilities of properties within the compositional design space, thereby allowing potentially attractive alloys for future applications to be defined and explored. Small quantities of C and B were added as grain boundary strengthening elements to reduce the impact of undesirable grain boundary defects (Refs. 31 and 32) that may be present in turbine blades and to provide tramp element control (Ref. 35). Hf was added to selected alloys at a nominal level of 0.2 wt% for oxidation resistance.

The slab castings measured approximately 15 cm long in the single crystal growth direction, 5 cm wide, and 0.6 cm thick. The castings were solution treated at a commercial heat treatment vendor. The solution temperature was reached by a series of step increments to avoid incipient melting and overshooting. Single crystal castings without Hf additions were solution treated for 6 h at 1315 °C, and castings with Hf were solution treated for 6 h at 1305 °C. Because of its lower solidus (Refs. 33 and 34), LDS-1110 was given a step heat treatment with a final solution temperature of 1288 °C for 18 h. Bulk chemical analyses (Table I) of the castings were obtained by inductively coupled plasma emission spectroscopy. Laue X-ray diffraction was performed on each slab to determine primary crystallographic orientation.

Prior to machining creep rupture specimens, castings were given a simulated coating cycle plus age. The simulated coating cycle was conducted in Ar at 1079 °C for 4 h and followed by Ar fan quenching. Aging was performed subsequently at 871 °C for 12 h, followed by Ar fan quenching to ambient temperature. These steps were applied because superalloy materials are typically used in a coated condition, and the 871 °C age has been used historically for g¢precipitation prior to service. Creep rupture specimens were then machined by low stress grinding with the axis of the specimen gage parallel to the single crystal growth direction. Threaded specimens had a nominal 3.175 mm gage diameter, 1.9 cm gage length, and 6.8 cm overall length. Constant load creep testing was performed in air according to ASTM-E 139-11 (Ref. 36) at temperatures of either 982 or 1093 °C. Creep extensometers were attached to V-notches on specimen shoulders, and temperatures were maintained to within ±2 °C along the specimen gage length.

TABLE I.—ANALYZED COMPOSITIONS (wt%) OF SINGLE CRYSTAL ALLOYS

| Alloy | Cr | Co | Mo | Re | Al | Ta | Hf | Y[a], ppm wt | Ni | B | C | S, ppm wt |
|---|---|---|---|---|---|---|---|---|---|---|---|---|
| LDS-0010 | 0.00 | 0.00 | 12.02 | 0.00 | 6.08 | 6.14 | 0.00 | 53 | balance | 0.0040 | 0.0140 | ---------- |
| LDS-0101 | 0.01 | 9.76 | 7.01 | 2.92 | 6.01 | 6.28 | 0.00 | 70 | balance | 0.0045 | 0.0098 | ---------- |
| LDS-5051 | 2.35 | 0.00 | 9.01 | 2.99 | 6.03 | 6.11 | 0.00 | 65 | balance | 0.0040 | 0.0140 | 2.8 |
| LDS-5555 | 2.43 | 4.91 | 9.48 | 1.48 | 6.03 | 6.17 | 0.00 | 46 | balance | 0.0032 | 0.0168 | 2.8 |
| LDS-4583 | 3.90 | 5.00 | 8.10 | 3.00 | 6.00 | 6.30 | 0.20 | 57 | balance | 0.0030 | 0.0104 | 2.8 |
| LDS-4183 | 3.93 | 9.97 | 8.13 | 3.04 | 6.05 | 6.22 | 0.20 | 73 | balance | 0.0030 | 0.0139 | 3.2 |
| LDS-4164 | 4.00 | 11.00 | 6.10 | 4.10 | 6.00 | 6.20 | 0.20 | 73 | balance | 0.0040 | 0.0110 | ---------- |
| LDS-1000 | 4.79 | 0.00 | 7.08 | 0.00 | 6.04 | 6.21 | 0.00 | 48 | balance | 0.0030 | 0.0098 | 3.1 |
| LDS-1501 | 4.93 | 4.98 | 7.13 | 3.05 | 6.01 | 6.26 | 0.19 | 57 | balance | 0.0030 | 0.0098 | ---------- |
| LDS-1101 | 4.70 | 9.90 | 7.10 | 3.00 | 6.00 | 6.20 | 0.00 | 50 | balance | 0.0035 | 0.0160 | 4.1 |
| LDS-1164 | 4.90 | 10.00 | 6.10 | 4.00 | 6.00 | 6.30 | 0.20 | 42 | balance | 0.0030 | 0.0130 | ---------- |
| LDS-1101+Hf | 5.00 | 10.00 | 7.30 | 3.10 | 6.10 | 6.50 | 0.19 | 79 | balance | --------- | 0.0240 | 0.87 |
| LDS-1182 | 4.88 | 9.99 | 8.19 | 2.03 | 5.99 | 6.25 | 0.22 | 66 | balance | 0.0040 | 0.0097 | ---------- |
| LDS-1110 | 4.68 | 9.76 | 11.95 | 0.00 | 5.98 | 6.08 | 0.00 | 47 | balance | 0.0030 | 0.0180 | ---------- |

[a]Analysis from top of slab

The g¢particle size was measured prior to creep testing in each alloy after the simulated coating cycle plus age. Transverse cross-sections of these single crystal slabs were metallographically polished and etched with 33% $CH_3COOH$, 33% $H_2O$, 33% $HNO_3$, and 1% HF, all by volume. Scanning electron microscopy (SEM) was used in the secondary electron imaging mode to obtain a minimum of five areas at magnifications of 10,000X for each alloy. Mean edge lengths from a minimum of 120 g¢particles in each alloy were obtained for the g¢size measurement. In addition, the spacings between the g¢rafts were measured for each alloy after creep rupture testing. For this measurement, the uniform portion of each specimen gage was re-heated to the testing temperature, held for 30 min, and then water quenched to ambient temperature. This re-aging step was performed to produce a microstructure representative of that at the test temperature, since creep ruptured specimens underwent a slow furnace cooling. Gage sections were prepared parallel to the applied stress direction to view and measure the thickness of the interlamellar, or g, spacing. The metallographic preparation and SEM techniques employed for this measurement were identical to those described for g¢size determinations. The techniques for measuring other key microstructural parameters, including g¢solvus, g¢volume fraction, g and g¢phase chemistries, volume fraction of TCP phases, and g - g¢lattice mismatch have been described in detail in earlier publications (Refs. 33 and 34). The g¢volume fraction, g and g¢phase chemistries, and volume fraction of TCP phases were obtained at the creep testing temperatures; the g - g¢lattice mismatch was measured at ambient temperature.

Regression models for estimating the creep rupture properties were developed using JMP 7.0 (SAS Institute Inc.). All candidate independent variables, A, were first normalized to lie between –1 and 1 using the relationship, $\mathbf{A}^* = (A - A_{mid})/(\Delta A/2)$, where **A*** is the normalized variable, $A_{mid}$ is the midpoint of the range of variable A, and $\Delta A/2$ is the half-range of variable A. Stepwise forward and reverse selections of significant terms were compared, with at least a 90 percent probability of significance necessary for inclusion of a term. This method allowed for the determination of the relative influence of specific microstructural parameters, as well as their interaction terms, on creep rupture life. Goodness of fit was assessed using both the coefficient of determination adjusted for the number of variables, $R^2_{adj}$, and the residual error for each fitted response which was estimated using root mean square of error, rmsE. Regression models were also developed to determine the influence of composition on creep. In earlier studies, we developed regression models for estimating the compositional effects on the various microstructural parameters described in the preceding paragraph (Refs. 33 and 34). A regression model was developed in this study for the initial g¢size before creep testing and was based on composition and other microstructural parameters.

# Results

## Initial g - g¢ Microstructure

In the present study, the g - g¢ microstructures were examined in all LDS alloys prior to creep testing. These initial microstructures were representative of each alloy after a standard heat treatment consisting of the solution treatment, simulated coating cycle, and g¢ precipitation age. The majority of the LDS alloys had cuboidal g¢ precipitates that were aligned along {001} directions, and a typical initial microstructure observed for these alloys prior to creep testing is shown in Figure 1(a) for LDS-1101.

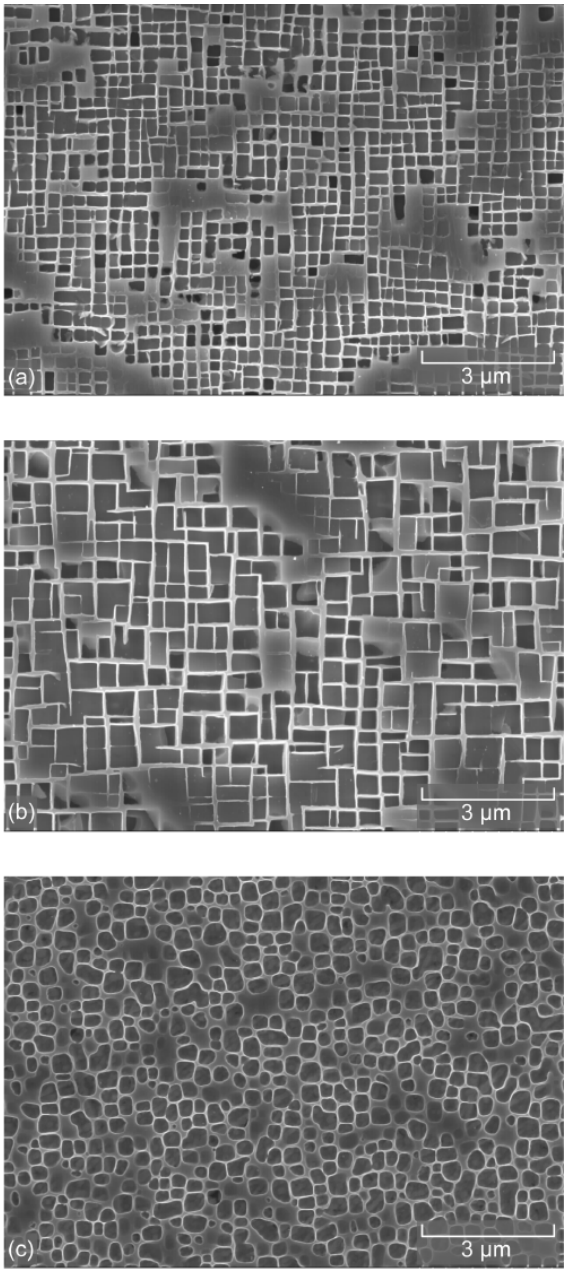


Figure 1.—Initial $\gamma - \gamma'$ microstructures prior to creep testing in selected alloys: (a) LDS-1101; (b) LDS-5555; and (c) LDS-0101. The microstructure for LDS-1101 is considered to be typical for most of the LDS alloys.

TABLE II.—MEASURED MICROSTRUCTURAL PARAMETERS

| Alloy | g¢size, mm | g¢volume fraction at 982 °C, vol% | g¢volume fraction at 1093 °C, vol% | g - g¢lattice mismatch, percent |
|---|---|---|---|---|
| LDS-0010 | 0.56 | 67.5 | 58.8 | –0.365 |
| LDS-0101 | 0.39 | 61.5 | 52.2 | +0.137 |
| LDS-5051 | 0.37 | 65.2 | 55.1 | –0.416 |
| LDS-5555 | 0.45 | 64.1 | 54.5 | –0.315 |
| LDS-4583 | 0.36 | 62.5 | 50.8 | –0.344 |
| LDS-4183 | 0.31 | 61.6 | 48.7 | –0.298 |
| LDS-4164 | 0.25 | 60.4 | 47.0 | –0.157 |
| LDS-1000 | 0.55 | 60.1 | 50.6 | 0 |
| LDS-1501[a] | 0.34 | 61.2 | 48.9 | –0.298 |
| LDS-1101 | 0.27 | 60.3 | 48.8 | –0.249 |
| LDS-1164 | 0.27 | 60.3 | 47.5 | –0.208 |
| LDS-1101+Hf | 0.33 | 61.0 | 48.1 | --------- |
| LDS-1182[a] | 0.33 | 60.9 | 48.1 | –0.244 |
| LDS-1110[b] | 0.71 | 64.0 | 50.4 | –0.539 |

[a]Not included in models; used as a verification alloy
[b]Not included in models due to TCP content

In contrast, LDS-5555 (Fig. 1(b)) and LDS-0010 exhibited sharp cuboidal g¢particles with some coarsening and coalescence evident; LDS-1110 exhibited a significantly coarsened microstructure with irregular-shaped precipitates. Rounded g¢particles were observed in LDS-0101 (Fig. 1(c)); this alloy had a positive mismatch at room temperature (Refs. 33 and 34).

Table II and Figure 1 show that the initial g¢size varied significantly from alloy to alloy. Ideally, g¢ size effects are studied by intentionally varying g¢size through aging studies. However, in the present work, the initial g¢size was simply measured for each alloy after the standard heat treatment was performed. It should be noted that LDS-1110 was solution treated at a lower temperature in a laboratory furnace with a slower cooling rate, while all other LDS alloys were solution treated in a batch in an industrial-sized furnace. Keeping the heat treatment temperatures close and cooling rates constant was not sufficient for maintaining a relatively constant g¢size among these alloys. Thus, the initial g¢size became a variable between the alloys in this work, and the regression model that was developed to estimate the initial g¢size will be described in a subsequent section.

## Creep Rupture Behavior

Creep rupture testing was conducted on the LDS alloys under the following conditions: 982 °C/ 241 MPa; 982 °C/207 MPa; 1093 °C/124 MPa; and 1093 °C/110 MPa. The rupture lives are listed in Table III. All single crystals tested had primary orientations within 8° of the [001]-orientation. Duplicate and triplicate tests under the same conditions for a given alloy indicated that the rupture lives were reproducible. A substantial range of rupture lives was attained over the composition space explored, which was desired and expected given the large changes in alloy content within the DOE. It was found that LDS-1101 was the most creep resistant at both stress levels at 982 °C. LDS-4583 and LDS-4183, which are derivatives of LDS-1101 with higher Mo levels and slightly lower Cr levels, were among the most creep resistant at 1093 °C. LDS-0101, LDS-1000, and LDS-1110 consistently exhibited weak creep properties under all testing conditions. LDS-0101 and LDS-1000 had low combined refractory contents of

TABLE III.—CREEP RUPTURE LIVES FOR SINGLE CRYSTAL ALLOYS

| Alloy | Life (h) at 982 °C/ 241 MPa | Life (h) at 982 °C/ 207 MPa | Life (h) at 1093 °C/ 124 MPa | Life (h) at 1093 °C/ 110 MPa |
|---|---|---|---|---|
| LDS-0010 | 79.0, 84.9, mean = 81.95 | 221.4 | 109.25 | 331.85, 438.6, mean = 385.23 |
| LDS-0101 | 40.9 | 144.55 | 35.2 | 54.55 |
| LDS-5051 | 158.15, 160.5, 183.85, mean = 167.5 | 342.3 | 204.75, 281.9, 295.55, mean = 260.73 | 432.85, 472.25, 514.0, mean = 473.03 |
| LDS-5555 | 177.1, 189.5, mean = 183.3 | 316.55, 342.8, mean = 329.68 | 316.85, 329.8, mean = 323.33 | 968.25, 756.55, mean = 862.4 |
| LDS-4583 | 216.2, 301.4, mean = 258.8 | 662.8 | 546.3, 562.2, 613.6, mean = 574.03 | 913.6, 1105.6, mean = 1009.6 |
| LDS-4183 | 248.35, 296.55, mean = 272.45 | 754.3 | 439.35, 453.1, 521.9, mean = 471.45 | 730.2, 893.15, 941.3, mean = 854.88 |
| LDS-4164 | 209.35 | 484.1 | 140.2 | 324.7 |
| LDS-1000 | 45.75 | 109.65 | 72.5 | 144.15, 150.5, mean = 147.33 |
| LDS-1501 | 231.6, 303.6, mean = 267.6 | 729.25 | 391.65, 422.85, 484.2, 542.8, mean = 460.38 | 984.35, 1022.5, mean = 1003.4 |
| LDS-1101 | 236.85, 255.35, 304.2, mean = 265.47 | 938.3, 832.8, mean = 885.55 | 259.25, 325.5, 342.95, mean = 309.23 | 630.95, 632.8, mean = 631.88 |
| LDS-1164 | 251.7 | 803.3 | 286.95, 303.45, mean = 295.2 | 620.7, 690.9, mean = 655.8 |
| LDS-1101+Hf | 180.15, 227.0, mean = 203.58 | 576.15 | 271.4, 333.7, mean = 302.55 | 696.6, 712.5, mean = 704.55 |
| LDS-1182 | 193.4 | 611.15 | 262.6, 339.7, mean = 301.15 | 655 |
| LDS-1110 | 22.45, 25.25, mean = 23.85 | 67.85 | 16.1, 16.9, mean = 16.5 | 42.5 |

Cr, Mo, and Re, and low creep rupture properties resulted. LDS-1110 had the highest refractory content of all the LDS alloys cast but was observed to be highly unstable (Refs. 33 and 34) with respect to TCP phases that formed during creep. Alloy trends observed for time to 1 percent creep strain and minimum creep rate were similar to those observed for rupture life.

Typical creep curves for testing at 982 °C at applied stresses of 241 and 207 MPa are shown in Figures 2(a) and (b), respectively, for LDS-1101. Consistent with tertiary creep behavior, much of the creep curve exhibited a progressively increasing creep rate, as seen at 241 MPa in Figure 2(c), and a pronounced primary creep regime was not evident when the entire creep curve was examined under these testing conditions. However, the short-time insets in Figures 2(a) and (b) show that LDS-1101 initially exhibited a sigmoidal primary creep regime at 982 °C, where very little creep strain was accumulated for the first 10 h. This was particularly evident at 241 MPa where an incubation-like region was evident after loading. Increases in creep strain occurred subsequently along with increases in strain rate. However, comparison of the strain rate plots in Figures 2(c) and (d) shows that after ~30 h at 241 MPa the strain rate *decreased* with *increasing* creep strain. A region of minimum creep rate at $2.6' 10^{-8}$/s, which lasted for about another 50 h, was exhibited before the strain rate began steadily increasing again until specimen failure. This overall behavior was different from the reported creep curves for CMSX-4 at 950 °C and 185 MPa (Refs. 1 and 4), where the strain rate increased monotonically with increasing creep strain through the test.

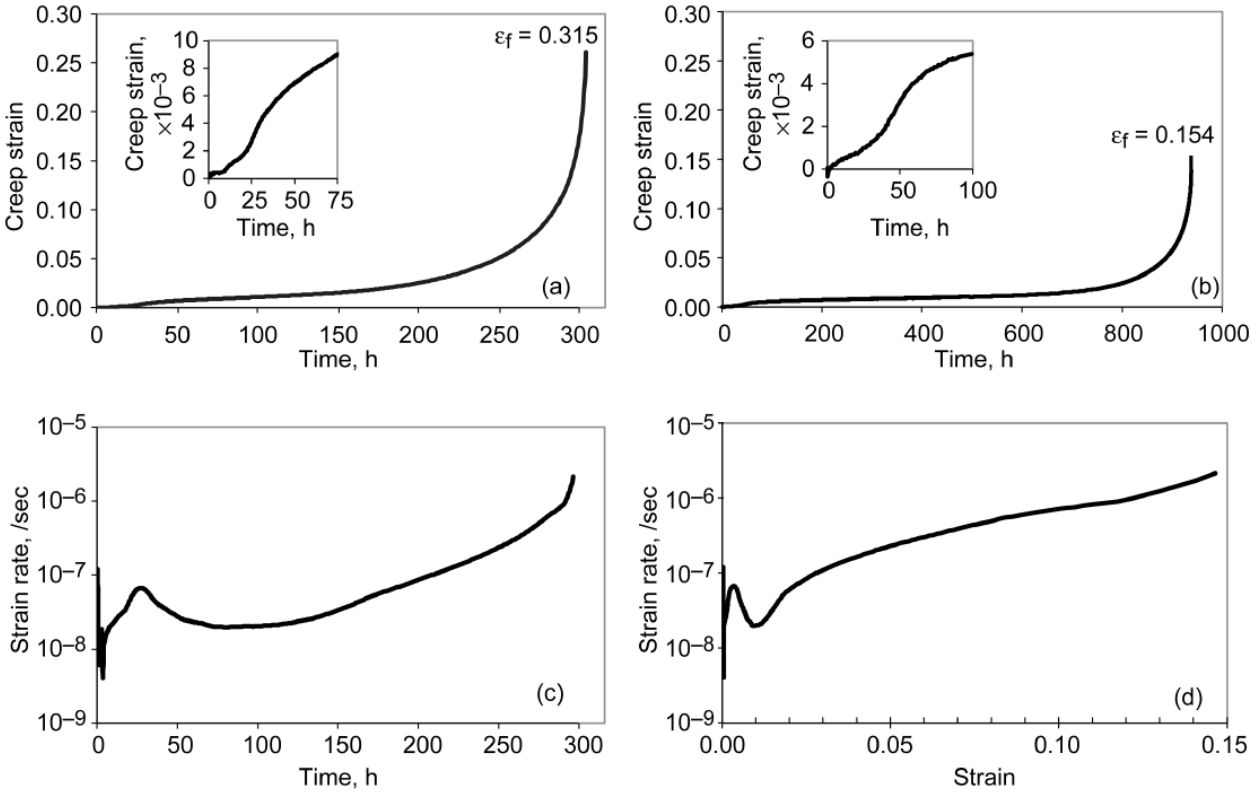


Figure 2.—Creep curves for LDS-1101 at 982 °C and applied stresses of (a) 241 MPa and (b) 207 MPa. Strain to failure is given by $\varepsilon_f$. Plots of (c) strain rate versus time and (d) strain rate versus strain are shown for LDS-1101 at 982 °C and 241 MPa.

The sigmoidal primary creep regime with a low initial strain accumulation was only observed for the more creep resistant alloys, which included LDS-5555, LDS-4583, LDS-4183, LDS-4164, LDS-1501, LDS-1101+Hf, LDS-1164, and LDS-1182, in addition to LDS-1101. The duration of the incubation-like region was seen to double as the applied stress at 982 °C was decreased from 241 to 207 MPa, and the extent of primary creep decreased as the applied stress decreased. These observations are consistent qualitatively with observations in the literature (Ref. 2). Additionally, the 4 wt% Re alloys displayed incubation periods at 241 MPa that were about double or triple the duration of those for the 3 wt% Re alloys and about eight times the duration of the incubation period for the 2 wt% Re alloy.

The characteristics of the creep curves at 1093 °C were different from those at 982 °C. Figures 3(a) and (b) display the typical 1093 °C creep curves at 124 and 110 MPa, respectively, for LDS-4583. At this temperature, three distinct stages of creep were easily identifiable, which is consistent with the high temperature rafting regime. A pronounced primary creep stage was observed up to creep strains of ~0.4 percent, as seen in the short-time insets in Figures 3(a) and (b). Then a rapid transition into a prolonged stage of low creep rates occurred over several hundred hours, which is evident in the plot of strain rate versus time in Figure 3(c). The region of minimum creep rate was followed by gradually increasing strain rates and then a rapid transition to high strain rates prior to failure. All LDS alloys at 1093 °C exhibited this overall creep behavior, except for LDS-0101. This weak alloy with low refractory metal contents exhibited tertiary creep behavior at 1093 °C. LDS-0101 exhibited a 2.5 h incubation-like period at 1093 °C/110 MPa, although an incubation period was not evident for this alloy at 1093 °C/ 124 MPa.

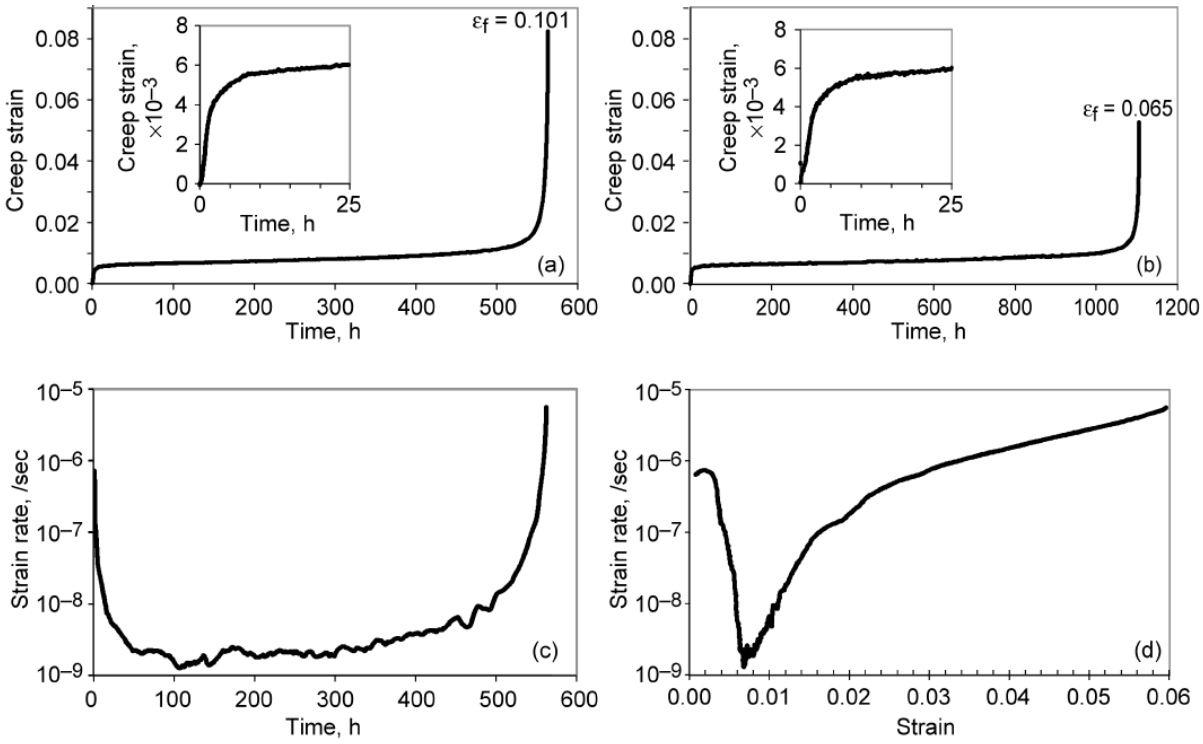


Figure 3.—Creep curves for LDS-4583 at 1093 °C and applied stresses of (a) 124 MPa and (b) 110 MPa. Strain to failure is given by $\varepsilon_f$. Plots of (c) strain rate versus time and (d) strain rate versus strain are shown for LDS-4583 at 1093 °C and 124 MPa.

It is interesting to note that all LDS alloys at 1093 °C, except LDS-0101, reached a minimum creep rate at a strain of ~0.007, Figure 3(d), which was equal to that observed in CMSX-4 at temperatures between 1050 and 1200 °C (Ref. 4). However, even after this critical creep strain was reached for the LDS alloys, much of the creep life remained, and the creep rate remained low for a prolonged period of time. This is in contrast to the behavior of CMSX-4 (Ref. 4), in which failure occurred within a few tens of hours after the critical strain of ~0.007 was reached. It should be mentioned that despite the pronounced primary creep stage, the time to 1 percent creep strain for the LDS alloys tended to be a large fraction of the creep rupture life at 1093 °C, typically ranging between 70 to 90 percent of the total life. The stronger LDS alloys at 982 °C also exhibited minimum creep rates at strains of ~0.007, which suggests that their 982 °C creep behavior was a blend of behavior of the high temperature rafting regime and the tertiary creep regime.

All LDS alloys in this study developed g¢rafting by the end of the creep rupture tests at both 982 and 1093 °C. Examples of the rafting are shown after creep testing at 982 and 1093 °C for LDS-5555 in Figures 4(a) and (b), respectively, and for LDS-0101 in Figures 4(c) and (d), respectively. The rafts formed perpendicular to the applied stress direction. It was evident by comparing the darker phase (g¢) in these micrographs that the g¢volume fraction was higher at 982 °C in both alloys. For LDS-5555, the g phase at 982 °C appeared as islands surrounded by the continuous g¢phase, whereas at 1093 °C, the microstructure more resembled that of alternating lamellae of each phase. For LDS-0101, the g¢phase was largely continuous but examples of discrete g¢rafts surrounded by g may be found at both temperatures. Although no interrupted creep tests were conducted prior to failure, it may be safely assumed that rafting occurred more rapidly at 1093 °C due to faster diffusion rates. Rafting in first-generation single crystal alloys was generally completed by the end of a primary creep regime (Refs. 11, 24, and 28). The shapes of the short term creep curves in Figures 2 and 3 also support more rapid rafting at 1093 °C due to the prominent primary creep regime exhibited by most alloys in this study.

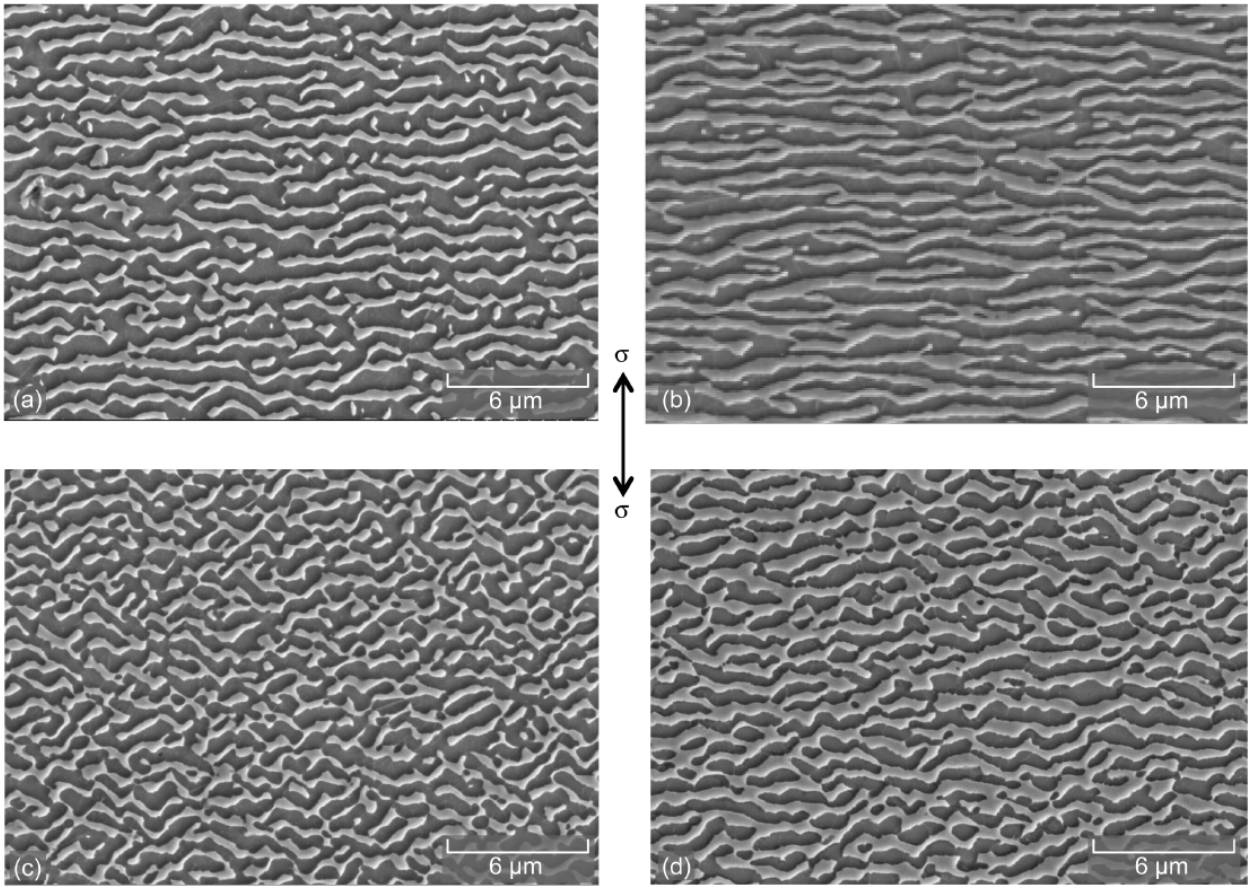


Figure 4.—Microstructures after creep rupture for: (a) LDS-5555 at 982 °C and 241 MPa; (b) LDS-5555 at 1093 °C and 124 MPa; (c) LDS-0101 at 982 °C and 172 MPa; and (d) LDS-0101 at 1093 °C and 124 MPa. The γ' phase is dark and the γ phase is light. Applied stress direction is indicated by σ.

## Effects of Composition on Creep Rupture Life

Regression models were developed for estimating the effect of bulk composition on rupture life at both applied stress levels at 982 and 1093 °C. The mean rupture life for each alloy under each testing condition and the analyzed bulk contents for Cr, Co, Mo, and Re in Table I were used in the multiple linear regression analyses. The best regression models generated for rupture life included the single element variable terms of Re, Mo, and/or Cr with interaction terms between some of the element variables; Co did not play a significant role. However, the regression model fits were less than satisfactory with $R^2_{adj}$ values less than 65 percent. Fits improved when the average logarithmic lives were used in the regression models; $R^2_{adj}$ increased to values between 64 and 82 percent depending on the test condition, but these values were still less than desired. An alternate approach was pursued where the compositional effects were indirectly accounted for through the changes they imposed on key microstructural parameters. Changes in alloy composition simultaneously affect numerous microstructural parameters, such as g¢solvus temperature, g¢volume fraction, initial g¢size, g - g¢lattice mismatch, g and g¢phase chemistries, solid solution strengthening, and TCP phase precipitation (Refs. 33 and 34).

## Effects of Microstructural Parameters on Creep Rupture Life

### g¢Volume Fraction

Although the g¢formers (Al and Ta) were intentionally held constant in the bulk alloys, the Cr, Co, Mo, and Re contents were varied in the DOE and were found to alter the g¢volume fraction (Refs. 33 and 34). Table II shows that the g¢volume fraction ranged from 60 to 68 vol% at 982 °C for the LDS alloy series. The amount of g¢phase decreased as the temperature increased. The LDS alloys exhibited g¢ volume fractions between 47 and 59 vol% at 1093 °C.

The mean creep lives are displayed as a function of the measured g¢volume fractions at 982 and 1093 °C in Figures 5(a) and (b), respectively. Figure 5(a) shows that an apparent peak in creep life at 982 °C/241 MPa occurred at g¢volume fractions between 60 and 62 vol%. It may be seen in this figure that the highest creep lives at 982 °C were associated with some of the lowest volume fractions of g¢that were observed at this temperature. However, there were weak alloys across the entire range of observed g¢volume fractions. Figure 5(b) displays the creep lives at 1093 °C and 110 MPa as a function of the g¢ volume fractions at that temperature. Here, the maximum in rupture life did not occur at the lowest measured g¢volume fractions, but instead occurred near 50 vol% g¢ Since g¢volume fraction at very elevated temperatures is often correlated with g¢solvus (Refs. 33 and 34), creep rupture lives were also examined as a function of g¢solvus temperature. However, no clear relationship between creep life and g¢ solvus was evident, in contrast to the work of Caron (Ref. 10).

### Initial g¢Size

The mean creep lives at 982 and 1093 °C are displayed in Figures 6(a) and (b), respectively, versus the initial g¢size obtained prior to testing. Figure 6(a) indicates that the creep rupture lives at 982 °C and 241 MPa generally increased with decreasing initial g¢size. A maximum in 982 °C creep life occurred in alloys with initial g¢sizes between 0.27 and 0.36 mm, although a range in creep life could be seen at any given initial g¢size. The weak alloys with lives under 100 h at 982 °C seemed insensitive to g¢particle size, since those alloys displayed a wide range of initial g¢sizes from 0.39 to 0.71 mm. Figure 6(b) indicates a maximum in creep life at 1093 °C and 110 MPa at an initial g¢size of ~0.35 mm; however, the relationship between g¢size and creep life was not as clear cut at 1093 °C.

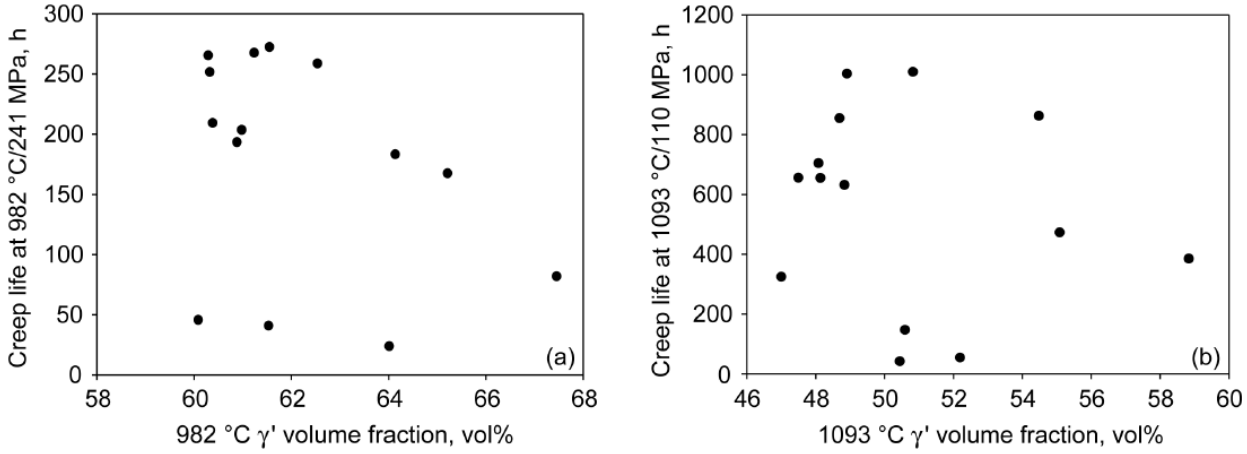


Figure 5.—Creep rupture life is shown for LDS alloys as a function γ' volume fraction at: (a) 982 °C and 241 MPa and (b) 1093 °C and 110 MPa.

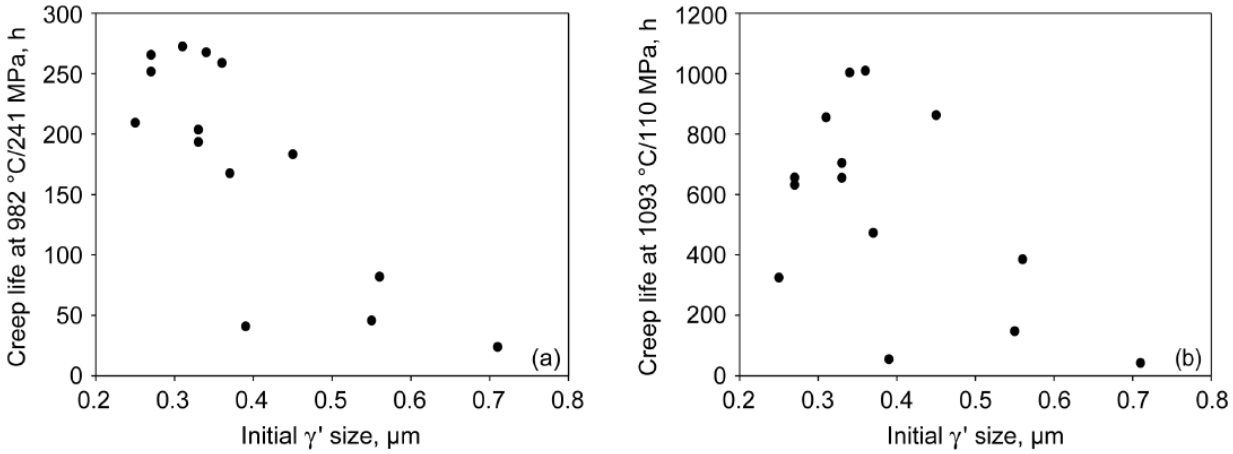


Figure 6.—Creep rupture life is shown for LDS alloys as a function of initial γ' size for: (a) 982 °C and 241 MPa and (b) 1093 °C and 110 MPa.

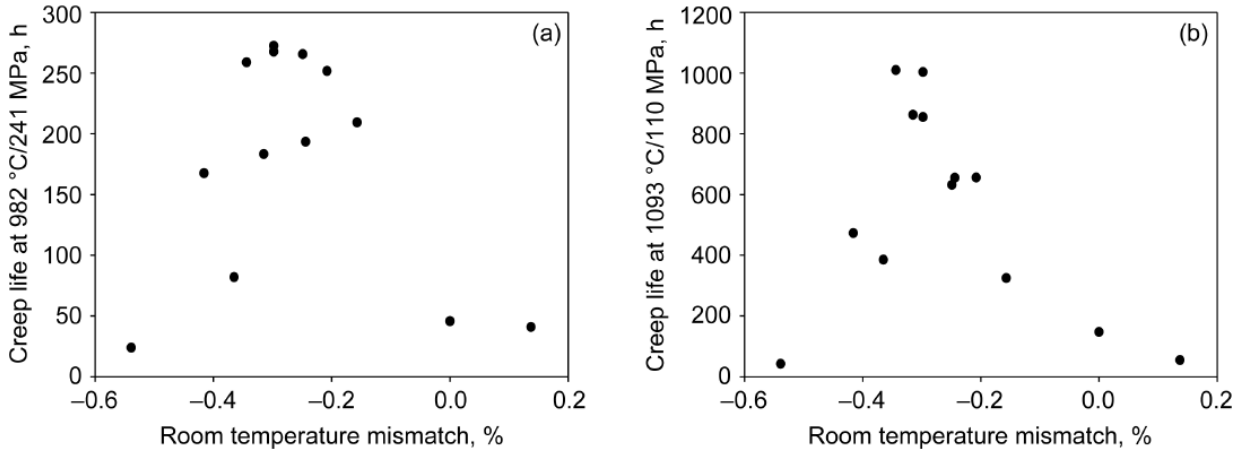


Figure 7.—Creep rupture life is shown for LDS alloys as a function of γ – γ' lattice mismatch for: (a) 982 °C/241 MPa and (b) 1093 °C/110 MPa.

### g - g¢ Lattice Mismatch

The unconstrained lattice mismatch d is defined as the magnitude of the elastic coherency strains between the g and g¢ phases and is given by (Ref. 37):

$$\delta = 2 (a_{\gamma'} - a_{\gamma}) / (a_{\gamma'} + a_{\gamma}) \quad (1)$$

Equation (1) defines negative mismatch as the case in which the g lattice parameter, $a_{\gamma}$, is larger than the g¢ lattice parameter, $a_{\gamma'}$. Table II shows that the LDS alloys cover a wide range of room temperature lattice mismatch from - 0.539 to 0.137 percent. However, the majority of the compositional space studied produced negative values of mismatch at room temperature due to the Cr, Mo, and Re contents that partition preferentially to the g matrix (Refs. 33 and 34) and increase the g lattice parameter.

Figures 7(a) and (b) show the mean creep lives obtained at 982 °C/241 MPa and 1093 °C/110 MPa, respectively, as a function of room temperature lattice mismatch. Figure 7(a) appears to display three tiers of creep lives at maximum, intermediate, and low levels at 982 °C and 241 MPa. The peak in creep rupture life at 982 °C occurred for alloys with levels of mismatch between - 0.34 and - 0.25 percent. Intermediate lives were exhibited by alloys spanning a wider range of mismatch, and close examination of

the alloys in the second tier showed that they also exhibited different g¢ volume fractions and initial g¢ sizes. For example, LDS-5555 appeared to have an optimum level of mismatch based on the peak position in Figure 7(a) but possessed a relatively high g¢ volume fraction of 64.1 vol% and a large initial g¢ size with both of these parameters outside the ranges observed for the peak lives in Figures 5(a) and 6(a). The three alloys with the lowest lives in Figure 7(a) exhibited extreme values of lattice mismatch, along with non-optimum values of other microstructural parameters. In contrast, the creep lives at 1093 °C and 124 MPa showed a narrow peak as a function of lattice mismatch, as seen in Figure 7(b), with the peak lives occurring at mismatch values between - 0.34 and - 0.30 percent. The apparent optimum range of lattice mismatch for these alloys appeared to be shifted toward slightly larger magnitudes at 1093 °C than at 982 °C.

It should be emphasized that although Figures 5 to 7 display apparent relationships between creep life and either g¢ volume fraction, initial g¢ size, or lattice mismatch, these plots may be somewhat misleading because the various microstructural features were changing simultaneously as the compositions were varied. Therefore, regression analyses were performed to sort out the relative influence of each key microstructural parameter on creep rupture life at 982 and 1093 °C.

## Microstructure-Sensitive Creep Models

Regression models were developed using the mean creep rupture lives (Table III) for testing that was performed at 982 °C/241 MPa, 982 °C/207 MPa, 1093 °C/124 MPa, and 1093 °C/110 MPa. Analyses for both linear life and log life were attempted initially; the resultant models had slightly improved fits with log life, which is a common form for treatment of creep data. The microstructural parameters that were included as input variables were lattice mismatch, g¢ volume fraction, the square and the square root of g¢ volume fraction, g¢ solvus, initial g¢ size, volume fraction of TCP phase, interlamellar, or g spacing between the g¢ rafts, and Re and Mo concentrations in the g phase. The best regression models generated for each of the testing conditions were the following:

$$\text{Log life at 982 °C/241 MPa} = 1.9216 - \mathbf{0.4595}\,\delta^{*} - \mathbf{0.1982}\,V^{*}_{\gamma'@982\,°C} - \mathbf{0.1856}\,\gamma'^{*} \quad (2)$$
$$\text{with } R^{2}_{adj} = 94.2 \text{ percent, rmsE} = 0.077 \text{ log h}$$

$$\text{Log life at 982 °C/207 MPa} = 2.3656 - \mathbf{0.3689}\,\delta^{*} - \mathbf{0.1701}\,V^{*}_{\gamma'@982\,°C} - \mathbf{0.2447}\,\gamma'^{*} \quad (3)$$
$$\text{with } R^{2}_{adj} = 87.4 \text{ percent, rmsE} = 0.114 \text{ log h}$$

$$\text{Log life at 1093 °C/124 MPa} = 2.0335 - \mathbf{0.5891}\,\delta^{*} - \mathbf{0.3238}\,V^{*}_{\gamma'@1093\,°C} \quad (4)$$
$$\text{with } R^{2}_{adj} = 83.8 \text{ percent, rmsE} = 0.155 \text{ log h}$$

$$\text{Log life at 1093 °C/110 MPa} = 2.3619 - \mathbf{0.6322}\,\delta^{*} - \mathbf{0.2627}\,V^{*}_{\gamma'@1093\,°C} \quad (5)$$
$$\text{with } R^{2}_{adj} = 86.9 \text{ percent, rmsE} = 0.144 \text{ log h}$$

where the log life is in log h for each testing condition, $\delta$ is the room temperature lattice mismatch in percent as defined by Equation (1), $V_{\gamma'}$ is the volume fraction of the g¢ phase in fractional form measured at the indicated testing temperature, and $\gamma'$ is the initial g¢ size in microns measured prior to testing. All of the microstructural variables are presented in their normalized forms, as indicated by the asterisks in the equations. The relationship for the normalized form was given in the Materials and Procedures Section; the midpoint and the half-range for each normalized parameter are presented in Table IV. Additionally, the g¢ volume fraction is in fractional form, and not in percent, in order to maintain the values of all the microstructural inputs in a similar numerical range. Models were also developed for time to 1 percent creep strain and no significant differences were observed with respect to the specific terms included in the model, although the resultant fits were not quite as good.

TABLE IV.—NORMALIZED MICROSTRUCTURAL PARAMETER STATISTICS

| Statistic | g size, mm | g′ volume fraction at 982 °C | g′ volume fraction at 1093 °C | g - g lattice mismatch, percent |
|---|---|---|---|---|
| $A_{MID}$, midpoint | 0.405 | 0.6377 | 0.52915 | –0.1395 |
| DA/2, half-range | 0.155 | 0.0368 | 0.05915 | 0.2765 |

It should be mentioned here that two alloys, LDS-1501 and LDS-1182, from the present study were not included in the regression models so that they could be reserved as independent verification alloys, which will be described later in this section. LDS-1110 was also not included in the regression models because it was the only alloy that precipitated a high volume fraction of TCP phases at both creep testing temperatures, and as a result, exerted a very strong influence on the resultant regressions. Inclusion of input parameters for LDS-1110 enabled a TCP phase volume fraction term to be incorporated in the creep models that were initially developed; however, these models were statistically unbalanced due to an inadequately distributed TCP phase content within the design space. Therefore, the data for LDS-1110 were removed as inputs for all subsequent creep life regression models, and the TCP phase term was no longer statistically significant. Earlier work (Refs. 33 and 34) similarly showed that valid regression models for estimating the volume fraction of TCP phases could not be produced from bulk composition inputs of this alloy series because most of the LDS alloys contained less than 1 vol% TCP phase.

Equations (2) to (5) demonstrate that simple and straightforward regression models can be used to explain the creep rupture lives. Three microstructural parameter terms (lattice mismatch, g¢ volume fraction, and initial g¢ size) were found to be statistically significant for estimating creep lives at 982 °C, and only two terms (lattice mismatch and g¢ volume fraction) were significant for creep at 1093 °C. The regression models show that creep lives at both temperatures increased with more negative values of lattice mismatch and lower g¢ volume fractions, and at 982 °C, lives also increased with decreasing initial g¢ size.

### 982 °C Regression Models

The 982 °C creep models for both applied stress levels in Equations (2) and (3) produced relatively high values of $R^2_{adj}$ and relatively low values of rmsE, which indicates good correspondence between the estimated and observed rupture lives. Figure 8(a) shows the creep lives estimated by the regression model in Equation (2) versus the actual mean creep lives obtained for each alloy at 982 °C and 241 MPa. The LDS alloys used in developing the model are represented by the solid symbols, and the solid line in the figure represents unity, or complete correspondence between estimated and actual lives. The figure demonstrates the very good fit provided by the regression model over the wide range of rupture lives observed. Very similar results were seen in the correspondence between estimated and actual creep lives at 982 °C and 207 MPa, as seen in Equation (3) and Figure 9. Thus, 87 to 94 percent of the variations in creep life at 982 °C can be explained by three microstructural parameters that are often measured in Ni-base superalloys: lattice mismatch, g¢ volume fraction, and initial g¢ size.

It was desirable to have an independent verification of the regression models to verify the accuracy of the predictions. If the regression models developed for the LDS alloys were also found to closely estimate the creep lives of Ni-base superalloys that were not used in the regression analyses, then the models may be considered to be more robust. Pertinent data in the literature served this purpose. Creep properties and corresponding measurements of lattice mismatch, g¢ volume fraction, and initial g¢ size were available for alloys such as TMS-64 (Ref. 38), 12.5 Mo (Ref. 13), and MC-2 (Refs. 9 and 39). Creep rupture lives at 982 °C and 241 MPa were determined for these verification alloys by interpolating their creep data to the conditions used in this study. The microstructural parameters were obtained directly from the above mentioned references, although the initial g¢ sizes were not typically provided and had to be measured

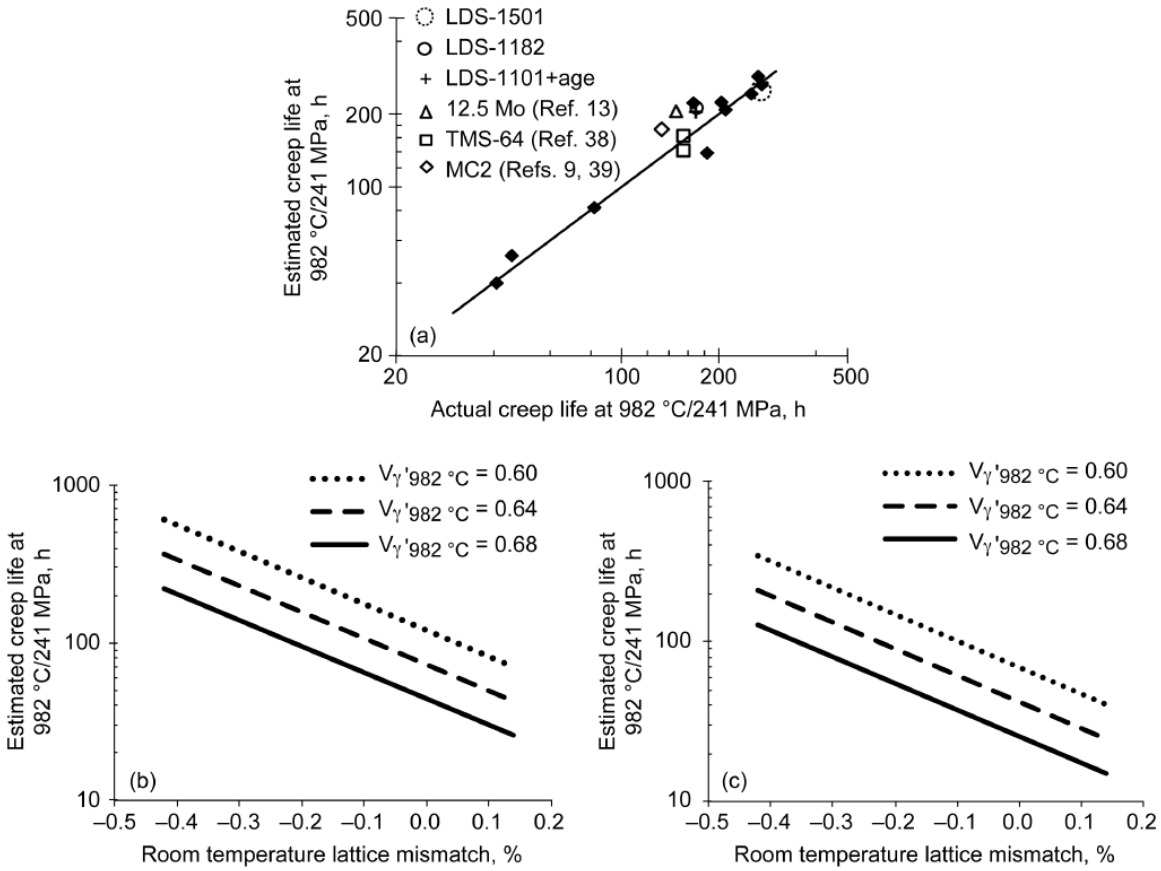


Figure 8.—(a) Estimated life from regression model for 982 °C and 241 MPa is plotted versus actual mean life for LDS alloys in this study (filled symbols). Lives for verification alloys, LDS-1501, LDS-1182, and LDS-1101+age, along those for alloys from the literature, are represented by the open symbols. Model output plots for estimated life at 982 °C and 241 MPa are plotted as a function of room temperature lattice mismatch and three levels of γ' volume fraction for initial γ' sizes of: (b) 0.25 μm; (c) 0.56 μm.

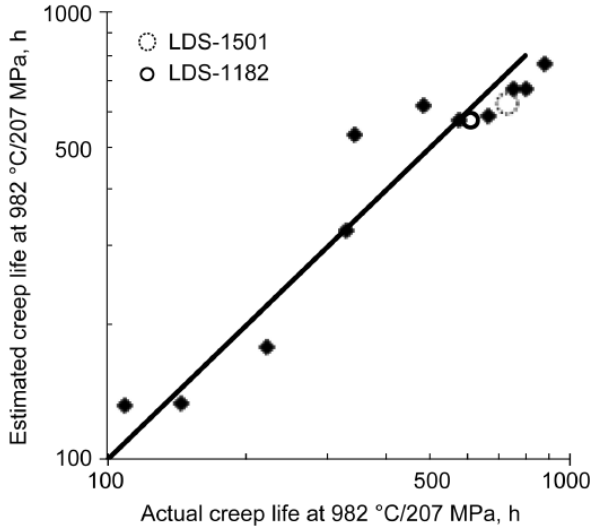


Figure 9.—Estimated life from regression model for 982 °C and 207 MPa is plotted versus actual mean life for LDS alloys in this study (filled symbols). Lives for verification alloys, LDS-1501 and LDS-1182, are represented by the open symbols.

from the published micrographs. In addition, three alloys from the present study, LDS-1501, LDS-1182, and LDS-1101+age, were not included in the regression models so that they could serve as independent verification alloys. LDS-1501 was selected for this purpose because it was consistently one of the strongest creep rupture alloys overall and was therefore believed to provide a robust test of the models. LDS-1182 was chosen because it exhibited intermediate lives and had a midrange bulk Re content. LDS-1101+age represents LDS-1101 with an additional high temperature age of 1121 °C for 4 h that coarsened the initial g¢size to 0.39 mm and decreased the creep life. The verification alloys are represented by the open symbols in Figure 8(a), where it may be seen that the regression model estimates for the verification alloys at 982 °C and 241 MPa were in good agreement with the experimentally determined creep lives. Similar results were obtained for 982 °C and 207 MPa, as seen in Figure 9. Thus, these verification alloys provided an independent confirmation of the creep models given in Equations (2) and (3).

For both stress levels at 982 °C, Equations (2) and (3) indicate that the rupture lives increased with more negative values of lattice mismatch, decreasing g¢volume fraction, and decreasing initial g¢size. The extent of the influence of the microstructural parameters on creep rupture life may be best explained by the regression model output curves in Figures 8(b) and (c), where the estimated creep lives at 982 °C and 241 MPa are shown as a function of lattice mismatch for three levels of g¢volume fraction at 60, 64, and 68 vol% and for a given g¢size. Figures 8(b) and (c) display the model output curves obtained for an initial g¢size of 0.25 and 0.56 mm, respectively. The values of the microstructural parameters displayed in Figures 8(b) and (c) cover the entire ranges observed experimentally at 982 °C.

Figures 8(b) and (c) demonstrate the very significant influence of lattice mismatch on creep lives at 982 °C and 241 MPa. Lattice mismatch increased the estimated creep life by a factor of 8.5, as this parameter was changed over its full range from 0.15 to - 0.42 percent at a given g¢volume fraction and particle size. The g¢volume fraction produced the next largest impact on rupture lives. *Decreasing* the g¢ volume fraction from 68 to 60 vol% *increased* the creep lives at 982 °C and 241 MPa by a factor of 2.7. Comparison of Figures 8(b) and 8(c) shows that decreasing the initial g¢size over the full range in this study from 0.56 to 0.25 mm increased the estimated creep life by a factor of 2.3. Thus, it may be seen that when changing the microstructural parameters over their full ranges in this study the lattice mismatch had the biggest impact on creep life at 982 °C and 241 MPa, followed by g¢volume fraction and lastly the initial g¢size. At the lower applied stress of 207 MPa, g¢size was found to have a slightly larger effect on rupture life than g¢volume fraction, but lattice mismatch was still observed to exert the strongest influence.

In an attempt to further explore creep models for 982 °C behavior, g¢solvus was substituted for g¢volume fraction as an input parameter. Since a high correlation existed between g¢solvus and g¢volume fraction, only one of these two microstructural parameters could be included in the models. However, the g¢volume fraction was found to be a better predictor overall at 982 °C. The interlamellar spacing between g¢rafts was employed as a regression input alternative to initial g¢size, but this spacing provided a slightly worse fit for the 241 MPa regression and was not found to be significant at 207 MPa.

### 1093 °C Regression Models

Equations (4) and (5) represent the creep models for both applied stress levels at 1093 °C. These regression models indicate that the 1093 °C rupture lives increased with more negative values of lattice mismatch and decreasing g¢volume fraction. The initial g¢size term was not found to be statistically significant at the higher creep testing temperature. It is not surprising that the creep models at 1093 °C have different regression terms from those at 982 °C, since the creep curves at these two temperatures exhibited distinctly different creep regimes. The 1093 °C creep models in Equations (4) and (5) produced values of $R^2_{adj}$ at 84 and 87 percent and values of rmsE of 0.15 and 0.14, respectively, for each applied

stress level, and Figure 10(a) shows the lives estimated by the regression model in Equation (5) versus the actual mean creep rupture lives obtained at 1093 °C and the lower applied stress level of 110 MPa. The LDS alloys used in developing the model are represented by the solid symbols, and the line in the figure represents unity. It may be seen in the figure that the regression model provides a good fit over the wide range of rupture lives observed by the LDS alloys. Fewer verification alloys were available for valid comparisons with the 1093 °C regression models. The alloys from the literature required extensive extrapolations to the creep testing conditions, did not have a complete set of microstructural data, or had compositions too dissimilar to our compositional space. Thus, verification alloys were limited to LDS-1501 and LDS-1182, which were shown by the open symbols in Figure 10(a) and were explained well by the creep model at 1093 °C and 110 MPa. Similar results were obtained for the creep model at 1093 °C and 124 MPa, as seen in Figure 11. Thus, much of the creep behavior at 1093 °C can be explained by lattice mismatch and g¢volume fraction.

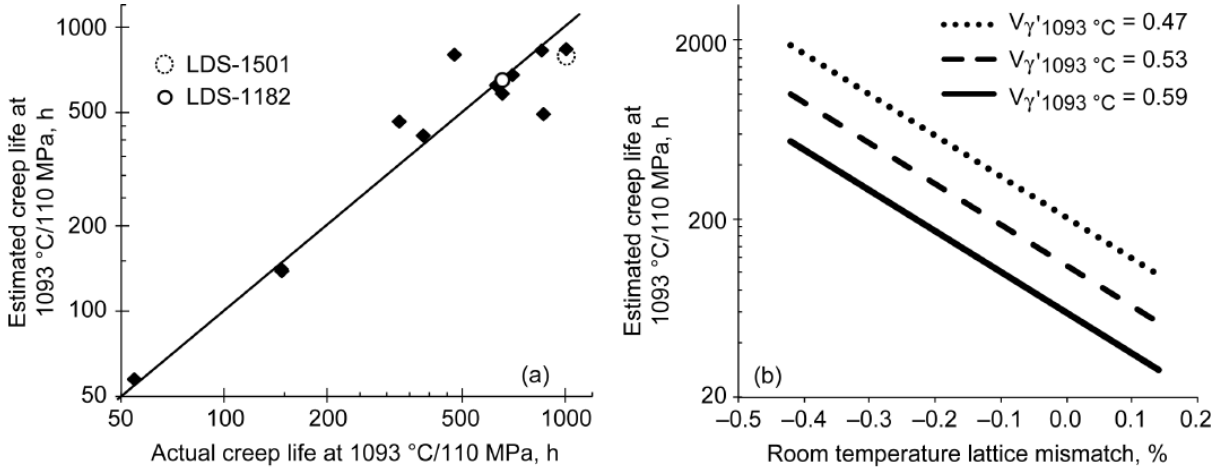


Figure 10.—Creep model results for 1093 °C and 110 MPa. (a) Estimated life from regression model versus actual mean life for LDS alloys in this study (filled symbols). Lives for verification alloys, LDS-1501 and LDS-1182, are represented by the open symbols. (b) Model output plots are shown for estimated life as a function of room temperature lattice mismatch and three levels of γ' volume fraction.

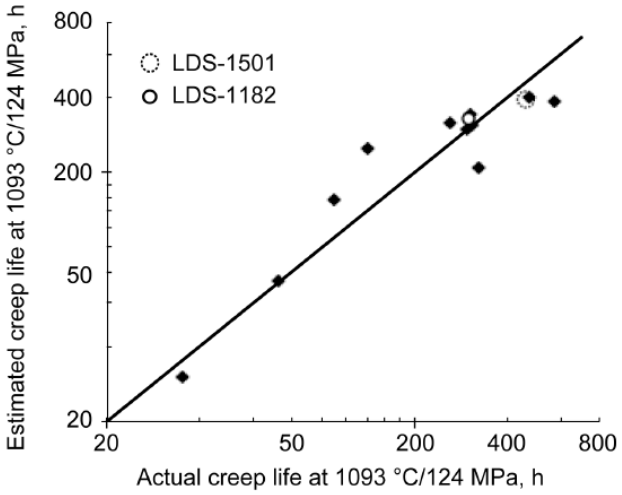


Figure 11.—Creep model results for 1093 °C and 124 MPa. Estimated life from regression model versus actual mean life for LDS alloys in this study (filled symbols) is indicated. Lives for verification alloys, LDS-1501 and LDS-1182, are represented by the open symbols.

The effects of lattice mismatch and g¢ volume fraction on 1093 °C creep rupture life are illustrated best by the regression model output curves. Figure 10(b) shows the model output curves for creep testing at 1093 °C and 110 MPa, where the estimated lives are shown as a function of lattice mismatch for three levels of g¢ volume fraction at 47, 53, and 59 vol%. This figure demonstrates the very strong influence of lattice mismatch on creep rupture life. Here, the estimated creep life was increased by a factor of 19.1, as lattice mismatch changed over its full range from 0.15 to - 0.42 percent at a given g¢ volume fraction. The figure also shows that decreasing the g¢ volume fraction from 59 to 47 vol% at 1093 °C improved creep life by a factor of 3.4, when the lattice mismatch was held constant. Similar effects of lattice mismatch and g¢ volume fraction were seen at 124 MPa. Thus, the g - g¢ lattice mismatch was the microstructural parameter observed to have the biggest impact on creep life at 1093 °C, whereas the g¢ volume fraction was statistically significant but had a much smaller effect.

Additional microstructural parameters were tested thoroughly for inclusion in the 1093 °C creep models in an effort to improve the accuracy of these models. However, none of these additional parameters were proven to be statistically significant. The g¢ solvus was substituted for g¢ volume fraction, however the solvus term was not statistically significant in these models for 1093 °C. The square of the g¢ volume fraction, as well as using the square root of the g¢ volume fraction, were substituted for the g¢ volume fraction term in an attempt to capture the apparent peak in creep behavior seen in Figure 5 and Reference 8; again, no improvements in the fit of the 1093 °C creep models resulted. The interlamellar spacing between g¢ rafts was also not found to be a significant factor. Perhaps this was not too surprising since this latter measurement was not obtained from tests interrupted at or near the observed minimum creep rate but instead was obtained after much creep deformation had ensued in the fractured specimens. The Re and Mo concentrations in the g phase were measured in earlier studies (Refs. 33 and 34) using phase extraction methods after aging at 1093 °C. Neither the Re nor the Mo concentrations in the g phase were found to be significant regression model terms at 1093 °C, although their effects were present indirectly through the lattice mismatch and g¢ volume fraction terms.

## Regression Model for Initial g¢ Size

The initial g¢ size prior to testing was observed to vary significantly from alloy to alloy. Further examination revealed that the initial g¢ size was strongly affected by the amount of Re in the bulk alloy. Figure 12 shows that the Re-free alloys had the largest initial g¢ sizes, whereas the alloys with the highest Re content of 4 wt% had small initial g¢ sizes. The very coarse g¢ size at 0.71 mm was measured in one of the Re-free alloys, LDS-1110. This alloy is considered an outlier, however, because its g¢ size was affected by being solution treated in a laboratory furnace with a significantly slower cooling rate from the solution temperature. The data for LDS-1110 was therefore removed from subsequent g¢ size analyses.

It is well known that additions of Re retard g¢ coarsening by lowering bulk diffusion rates in Ni-base alloys (Ref. 40), and the overall behavior displayed in Figure 12 is consistent with that effect. However, the figure also shows variations in initial g¢ size at 3 wt% Re and an unexpectedly low initial g¢ size at 2 wt% Re, so bulk Re content is not the only factor affecting initial g¢ size. Other microstructural parameters, including g¢ solvus and g - g¢ lattice mismatch, are also expected to affect initial g¢ size. Therefore, the following regression model was developed to determine the relative effects of key microstructural parameters on initial g¢ size:

$$g_1' = 0.4163 - \mathbf{0.0998}\ Re^{*} + \mathbf{0.0772}\ g_s'^{*} + \mathbf{0.0389}\ d^{*} \qquad (6)$$

with $R^2_{adj}$ = 94.1%, rmsE = 0.0256 mm

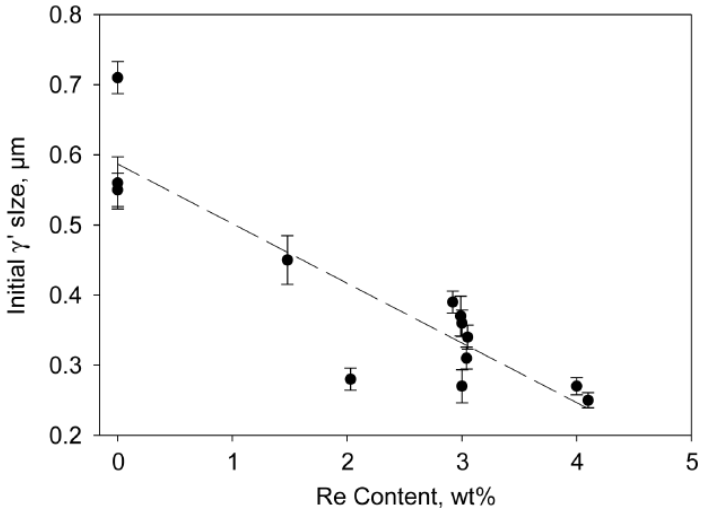


Figure 12.—Initial γ' size as a function of bulk Re content in wt%. Error bars indicate 95 percent confidence intervals.

where g¢is the initial g¢size is in mm, Re is the bulk content of that element in wt%, g¢ is the g¢solvus temperature in °C, and d is the g - g¢lattice mismatch in percent as defined in Equation (1). The terms with asterisks in Equation (6) represent the normalized form of each significant term, which is defined as the difference between the measured microstructural parameter and the midpoint of the range measured for that parameter, divided by the half-range of that parameter. Therefore, $Re^{*}$ = (Re – 2.05)/2.05, $g¢^{*}$ = (g¢ – 1278)/31, and $d^{*}$ = (d – (- 0.1395))/0.2765. This normalized approach standardizes each variable to a normalized range of –1 to 1 and allows the relative effect of each parameter term to be ranked over its entire range according to the magnitude of its coefficient shown in **bold** font in the equation.

The initial g¢size model in Equation (6) produced an excellent fit of the data based on the high values of $R^2_{adj}$ and low values of rmsE. An example of the correspondence between the g¢size estimated by the model and the experimentally determined g¢size is seen in Figure 13(a) over a wide range of g¢sizes. The solid line in the figure represents unity, or complete correspondence between estimated and measured g¢sizes. The coefficients of the terms in Equation (6) indicate that Re has the strongest effect on initial g¢size, and increasing Re reduces the initial g¢size. The g¢solvus and the lattice mismatch also have significant influences on initial g¢size, although their effects are smaller compared to that of Re additions.

The regression model output curves in Figures 13(b) and (c) may best clarify the relative effects of these microstructural parameters on initial g¢size. Figure 13(b) shows the potent influences of bulk Re content and g¢solvus temperatures on initial g¢size, with the lattice mismatch held constant at its mid-range level of - 0.1395 percent. The figure shows that the initial g¢size decreased by 0.19 mm as the Re content increased from 0 to 4 wt% at a given g¢solvus temperature. The figure also shows that the initial g¢size decreased by 0.15 mm as the g¢solvus temperature was decreased over its full range in this study from 1309 to 1247 °C. Figure 13(c) shows that the initial g¢size was reduced by a smaller amount, 0.08 mm, as the lattice mismatch changed over its full range in the study from 0.137 to - 0.416 percent.

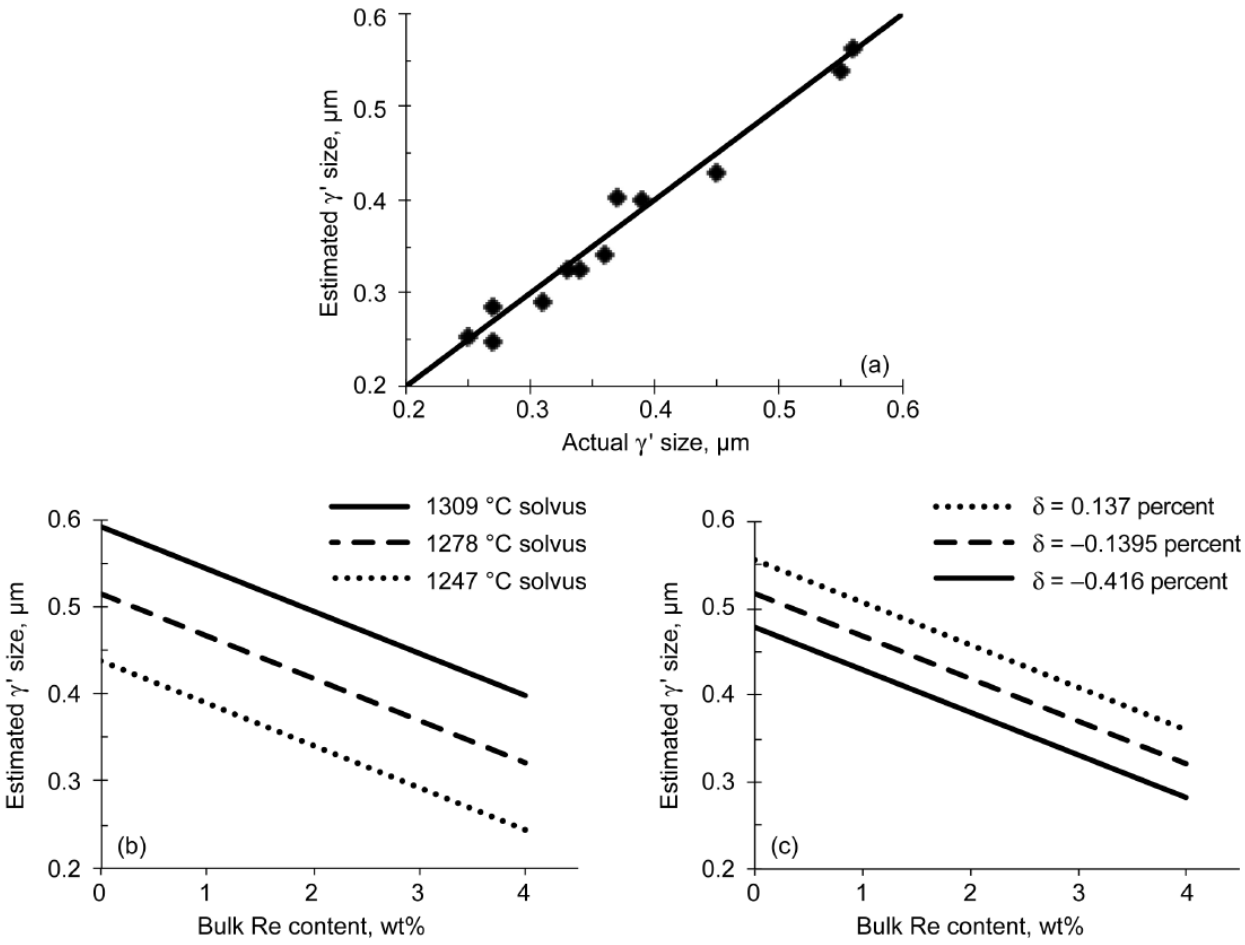


Figure 13.—(a) Initial γ' size estimated from microstructural parameter regression model fits the actual data well. All LDS alloys except LDS-1110 are included in this regression model. Model output curves for initial γ' size show the influence of: (b) bulk Re content and γ' solvus temperatures with lattice mismatch, δ, held at mid-range level of –0.1395 percent; and (c) bulk Re content and lattice mismatch with γ' solvus temperature held at mid-range level of 1278 °C.

# Discussion

## Creep Behavior

In the tests exhibiting sigmoidal creep at 982 °C, little or no creep strain accumulated during the first few hours. This behavior was reminiscent of incubation periods which are present as dislocations for the operative creep deformation mechanism are being generated (Refs. 2 and 41). It is interesting to note that when the applied stress level at 982 °C was substantially reduced to 138 MPa, the creep curve of a Re-bearing alloy, LDS-1501, exhibited the classic three creep regimes, as seen in Figure 14. The shape of this long-term creep curve at 982 °C was identical in shape to the creep curves typically observed at 1093 °C. This change in behavior at 982 °C was predicted in the temperature versus applied stress plot that summarized operative deformation modes for CMSX-4 (Refs. 1 and 2). The low applied stress level at 982 °C enabled a prominent primary creep regime to occur, which was followed by a lengthy secondary creep regime.

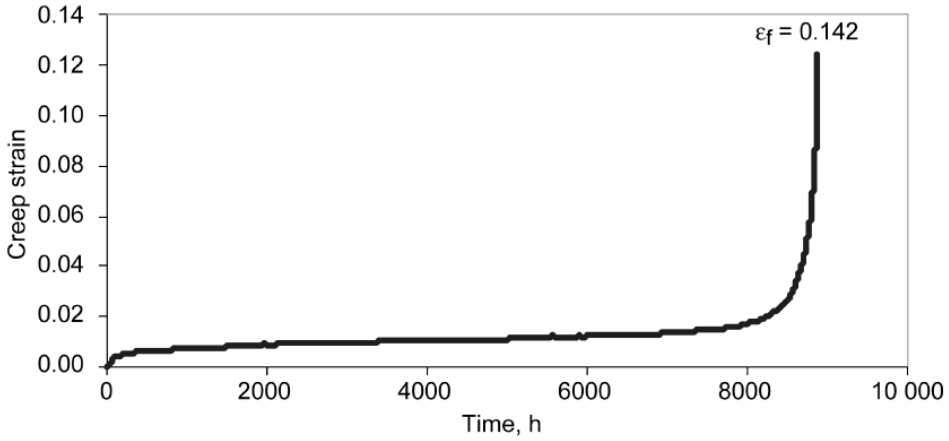


Figure 14.—Long-term creep curve for LDS-1501 at 982 °C and an applied stress of 138 MPa. Strain to failure is given by $\varepsilon_f$.

Tertiary creep behavior has been associated with slower g¢rafting kinetics in 3 wt% Re alloys (Ref. 4), whereas the high temperature creep behavior (~1000 to 1150 °C) is usually associated with rapid rafting. However, all LDS alloys in this study developed g¢rafting by the end of the creep rupture tests at both temperatures: during the tertiary or the modified tertiary creep behavior at 982 °C; and during the three regimes of creep observed at 1093 °C. The rafts in all alloys formed perpendicular to the applied stress direction. This includes LDS-0101, which had a room temperature mismatch of 0.137 percent; the mismatch of this alloy is likely to be close to zero at the creep testing temperatures. It is not known when the rafted structures in the LDS alloys became prominent or fully formed during creep, since interrupted creep tests were not conducted and all microstructural evidence was obtained after rupture. The lateral development of rafting did not appear to be appreciably different after rupture at 982 and 1093 °C in any given LDS alloy, although the rafts had a more wavy appearance in LDS-0101 (Ref. 34), likely due in part to its initially rounded g¢morphology and more random distribution within the matrix. It can be safely assumed that rafting was more rapid at 1093 °C than at 982 °C due to faster diffusion rates at the higher temperature. The short term creep curve in Figure 3 is also consistent with more rapid rafting at 1093 °C, since alloys have exhibited rapid rafting concurrent with a prominent primary creep regime (Ref. 24). This is also consistent with the observation that rafting is sluggish until some limited amount of deformation occurs and dislocations are produced (Ref. 42).

## Creep Regression Models

Lattice mismatch was observed to have a particularly strong effect on rupture life, based on the creep regression models at both creep testing temperatures. The influence of lattice mismatch is likely through the densely-spaced interfacial dislocation networks that provide a stronger barrier to penetration by deformation dislocations. The interfacial dislocation network arrays also have a role in stabilizing the g - g¢rafted structure against coarsening (Refs. 43 and 44). Varying the mismatch over the full range in this study from positive to negative values increased the estimated creep life by a factor of 8.5 at 982 °C and by a factor of 19.1 at 1093 °C. It is noteworthy that the influence of lattice mismatch was stronger at 1093 °C, where rafting was likely more rapid.

Although the high temperature mismatch is expected to be strongly correlated to the lower temperature value, it is possible that the models could be fine-tuned if lattice mismatch was measured at the creep testing temperatures. The g¢phase typically has a smaller thermal expansion coefficient than that of the g matrix (Ref. 14) in Ni-base superalloys, and as temperature is increased, the lattice parameter of the g phase increases more than that of the g¢phase. Empirical results from high temperature X-ray

diffraction show that the magnitude of the lattice mismatch in Ni-base superalloys changes by a small amount from the room temperature measurements. For example, a change in the magnitude of lattice mismatch of no more than 0.1 percent was measured in Re-free alloys from room temperature to 1000 °C (Ref. 14), and alloys with higher refractory metal content exhibited lower thermal expansion coefficients for both the g and g¢ phases. Other studies (Ref. 17) showed a change in the magnitude of lattice mismatch of up to 0.2 percent in Re-free alloys and up to 0.12 percent in Re-bearing alloys from room temperature to 1000 °C.

In this alloy design, lattice mismatch may also be considered an indirect indicator of solid solution strengthening because the refractories that were varied partitioned to the g phase (Refs. 33 and 34). Thus as the refractory metal contents were increased in the bulk, the lattice parameter of the g phase expanded and the mismatch became increasingly negative as solid solution strengthening increased simultaneously in the g matrix. Thus, the potential role of g phase compositions was explored in the creep models, particularly at 1093 °C, where the volume fractions of the g phase increased as the g¢ volume fractions began to drop more significantly (Refs. 33 and 34). Additionally, since the fits of the 1093 °C models were not quite as good as those at 982 °C, it was postulated that some other microstructural parameter was needed to better capture the creep behavior at the higher temperature. Thus, the concentrations of both Re and Mo in the g phase were considered as possible input terms to the 1093 °C creep regressions; however, these terms were not found to be statistically significant in the creep regression analyses. Other means of accounting for the solid solution content of g were also examined. For example, values for the effective diffusion coefficient were calculated by the method described in Zhu et al. (Ref. 3), who found a strong correlation between this coefficient and creep strength. However, no such correlation was found in the present study, and regression models did not benefit from inclusion of this parameter.

Substitutions of Mo for Re were made between LDS-1182, LDS-1101, and LDS-1164. As seen in Table I, these alloys had Mo contents from 8 to 6 wt% with a corresponding change in Re content from 2 to 4 wt%. This constitutes a maximum difference of 1.3 at% Mo and 0.65 at% Re between LDS-1182 and LDS-1164. Figure 15 displays the creep lives for the three above mentioned alloys as a function of bulk Re content. As seen by the open symbols in the figure, these alloys had very comparable lives at

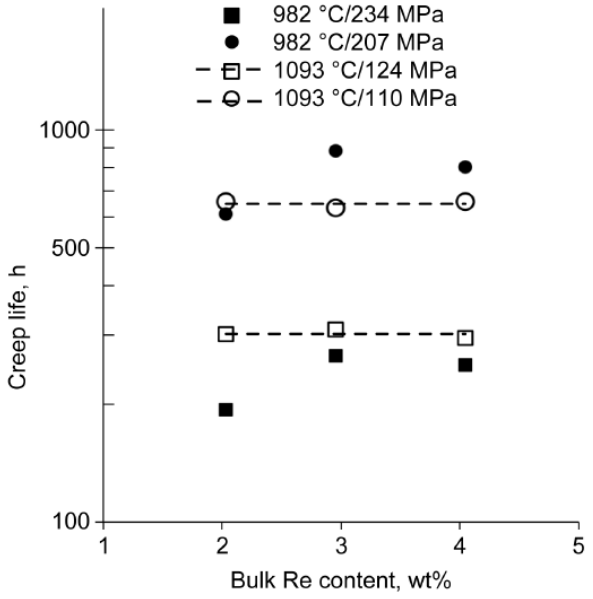


Figure 15.—Effect of substitutions of bulk Re content for equivalent Mo content (in wt%) on rupture lives at 982 and 1093 °C. Re additions of 2 wt% were sufficient for creep improvements at 1093 °C, but Re additions of 3 wt% were needed at 982 °C.

1093 °C, such that substitutions of Mo for Re, or Re for Mo, could be made without any creep deficit at this temperature. However, the behavior was different at 982 °C, as indicated by the filled symbols in Figure 15. Here, increasing Re content from 2 to 3 wt% with a concurrent decrease in Mo from 8 to 7 wt% improved creep life by about 38 percent. However, no additional benefits in creep life were obtained when Re was increased further from 3 to 4 wt% with a concurrent decrease in Mo from 7 to 6 wt%. Thus, it appears that 2 wt% Re was sufficient for creep improvements at 1093 °C, but 3 wt% Re was needed at 982 °C.

The present study shows the surprising result that lower g¢volume fractions are actually preferred for higher creep lives at both 982 and 1093 °C. This conclusion arises from the regression analyses used to estimate the individual contributions of each microstructural feature, which led to a linear term for the volume fraction effect as the best fit to the experimental data. It is expected that in fact the trends in Figures 8(b), (c), and 10(b) would not extend indefinitely to lower g¢volume fractions, but instead would show a peak at an optimum value. The model output curves indicate that this optimum is no higher than ~60 vol% at 982 °C and ~47 vol% at 1093 °C. These g¢volume fractions are much lower than those found in the relatively few g¢volume fraction studies performed (Refs. 1 and 8) and in other works that tend to promote optimum g¢volume fraction values as high as 65 to 70 percent (Refs. 1, 45 to 48). The trend observed in the present study between g¢volume fraction and creep life is consistent with that of Caron et al. (Ref. 9), who proposed that a topological inversion of the g¢phase occurred earlier during creep in alloys with g¢volume fractions greater than 50 vol% and that this morphological change lead to the onset of third-stage creep. The reasons for these discrepancies in the literature are still uncertain, but it is worth noting that the density of g - g¢interfaces in a rafted structure is maximized at 50 vol% g¢for a given g¢size. Thus, the trend between g¢volume fraction and creep life in the present study can be rationalized with respect to maximizing the number of g - g¢interfaces, which has been correlated with increased creep strengthening (Ref. 12).

The regression models did not predict a peak at ~50 vol% g¢since only linear input terms were statistically significant. To improve upon the creep models and to bound the lower end of g¢volume fractions, more alloys with g¢volume fractions lower than 50 vol% at 1093 °C need to be incorporated in the design space, combined with alloys having large negative values of mismatch as well as positive values of mismatch. Additionally, only the g-formers were varied in the DOE so it would be interesting to determine if this inverse relationship between g¢volume fraction and creep life holds if g¢formers are varied in the alloy design.

It should be noted that a discussion of an optimum g¢volume fraction is dependent on accurate measurements that are representative of the creep testing temperature. In our experience, accuracy is enhanced by using samples with lamellar g¢structures, rather than g¢cuboids, and by ensuring a rapid quench from the creep testing temperature. Additionally, systematic errors can be introduced by examination of etched samples via SEM. Etchants which remove g and leave g¢standing out on the surface will tend to overemphasize g¢volume fraction values if the interfaces are not perfectly perpendicular to the polished surfaces. Likewise, etchants which remove g¢will tend to underestimate g¢ volume fraction.

Regression analyses in the present study showed that the g¢size effect was significant at 982 °C, where finer g¢sizes improved creep lives. Ma et al. have suggested (Ref. 2) that deformation in the horizontal g channels is expected to dominate when the g - g¢interfaces are coherent early in tertiary creep. Creep deformation models for tertiary creep behavior at 950 °C (Ref. 2) predict improved creep resistance and increasing creep lives with decreasing g channel thickness at a constant g¢volume fraction. This outcome appears to be consistent with the results of this study, since g¢size is proportional to interparticle spacing at a constant g¢volume fraction. In addition, it should be mentioned that the initial g¢ size term in our creep regressions needs to be bounded on the low end; this could be accomplished by

incorporating finer g¢microstructures through the use of faster cooler rates from the solution temperature with and without subsequent aging treatments prior to testing.

Given the earlier studies (Refs. 11, 12, 23, and 24) where the initial g¢size had such a significant effect on subsequent rafting and resultant creep properties, it is unclear why the g¢size in this study was not found to be a significant factor for the creep models at 1093 °C. It is possible that the potent influences of lattice mismatch and g¢volume fraction overwhelmed any effect exerted directly by the relatively narrow range of initial g¢size. Since the microstructures were undoubtedly changing rapidly under stress as rafting developed, the g¢phase may have no longer resembled the initial g¢size, particularly at 1093 °C where the g¢volume fraction was lower. Interrupting the tests during the early stages of creep may shed some light on this. As a first step toward separating effects of g¢size from the simultaneous changes of other microstructural parameters, a single alloy (LDS-1101) was given an additional aging step to produce a larger initial g¢size of 0.39 mm. Creep testing this aged material at 1093 °C and 124 MPa reduced its rupture life by 24 percent. Thus, the effect of g¢size does appear to be present at 1093 °C based on these limited testing data, at least for LDS-1101.

## Effect of Topologically Close Packed Phases

It is clear that high quantities of TCP phases adversely affect creep and need to be taken into account in a microstructure-sensitive creep model. Because most alloys in this study were stable with respect to TCP phase formation, a TCP term was not included in the models presented here. To improve and expand upon these models, multiple LDS alloys that are more prone to precipitating higher levels of TCP phase would need to be tested and incorporated into a new creep model. This would also help to determine an upper limit for a tolerable amount of TCP phase in this design space.

It is generally believed that a TCP phase content £1 vol% is acceptable (Refs. 32 to 34). Single crystal alloy MC2 showed a reduction in minimum creep rates at 1010 °C with increasing TCP phase contents up to 0.85 vol%, but faster creep rates were observed with a higher TCP phase content of 1.05 vol% (Ref. 26). Earlier work by the present authors (Refs. 33 and 34) showed two alloys within the LDS design space that precipitated TCP phases during 1093 °C creep testing in quantities higher than commonly accepted amounts. One of these alloys (LDS-5051) was included in the creep models shown in Equations (4) and (5), although this alloy precipitated a mean TCP content of 2.39 vol% during 1093 °C testing. The other alloy (LDS-1110) was not included in the models because it exhibited a significantly higher TCP phase content of 5.55 vol% after 1093 °C creep testing (Refs. 33 and 34).

Figures 16(a) and (b) display the difference in hours between the actual creep lives and the creep lives estimated by the regression models (Eqs. (4) and (5)) for each LDS alloy tested at 1093 °C/124 MPa and 1093 °C/110 MPa, respectively. The differences in life in Figure 16 are shown as a function of the TCP phase content that was measured after creep testing. The alloys that were used as inputs for the creep models are indicated by the solid symbols in Figure 16. The open symbols represent the LDS alloys that were not included in the creep models; for these alloys, their measured microstructural parameters were inputted into Equations (4) and (5) to determine an estimated life. Figures 16(a) and (b) show that most of the alloys tested at 124 and 110 MPa, respectively, had life deviations that were clustered around 0 h. In contrast, LDS-1110 exhibited very large, negative deviations between actual and estimated lives of - 1031 h at 124 MPa and - 2386 h at 110 MPa. These deviations for LDS-1110 were attributed to its TCP phase content being so far outside the observed range in this study that the models significantly overestimated its creep lives at 1093 °C. In contrast, LDS-5051 was incorporated into the 1093 °C creep models, although the alloy precipitated a mean TCP content of 2.39 vol% during testing. Figure 16(a) shows that LDS-5051 exhibited a small deviation of - 58 h between actual and estimated creep life at 124 MPa which was within the scatter band observed for the other LDS alloys having up to 1.2 vol% TCP phase. However, at 1093 °C and the lower stress of 110 MPa, the life deviation for LDS-5051 increased

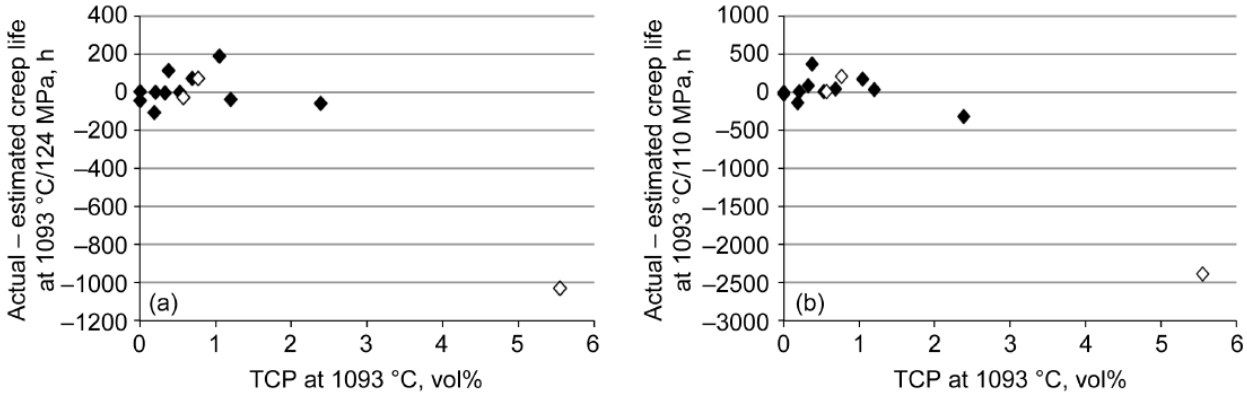


Figure 16.—Effect of topologically closed packed (TCP) phase content on differences between actual and estimated creep lives at 1093 °C at (a) 124 MPa and (b) 110 MPa. Closed symbols represent alloys included as inputs for the creep regression models in Equations (4) and (5), whereas open symbols indicate alloys that were not included as inputs for the creep regression models.

to - 318 h, which may indicate that this alloy was near the limits of an acceptable amount of TCP phase. This suggests that a TCP content of up to ~2 vol% may be tolerable under testing conditions where shorter creep lives of ~200 to 300 h are expected, but that a TCP content of ~2 vol% is not acceptable at lower stress levels where the lives are expected to be longer.

## Conclusions

1. Creep testing conducted at 982 °C produced modified tertiary creep curves with a sigmoidal-shaped primary stage. Creep tests at 1093 °C exhibited the three classic stages of creep. Directional coarsening of the g¢phase, or g¢rafting, was observed in all alloys at both temperatures.
2. The variation in creep lives among fourteen different alloys could be explained with regression models containing relatively few microstructural parameters. At 982 °C, g - g¢lattice mismatch, g¢ volume fraction, and initial g¢size were statistically significant in explaining the creep rupture lives. At 1093 °C, only lattice mismatch and g¢volume fraction were statistically significant. These models could explain from 84 to 94 percent of the variation in creep lives, depending on test condition.
3. The g - g¢lattice mismatch was the most potent variable in the microstructure-sensitive creep models. Creep life increased with increasingly negative lattice mismatch. The influence of lattice mismatch is likely through the densely-spaced interfacial dislocation networks that provide a stronger barrier to penetration by deformation dislocations, although the effect of solid solution strengthening of g cannot be separated from mismatch in this alloy series.
4. Creep lives increased with g¢volume fractions that were at or near the *low* end of the range of g¢ contents observed at each temperature, which was ~60 vol% at 982 °C and ~47 vol% at 1093 °C. It was argued that an optimum g¢volume fraction should be present near 50 vol%, as this maximizes the number of g - g¢interfaces in the rafted structure.
5. Using the variation in g¢size that developed upon cooling after heat treatment in the various alloys, it was found that a refinement of g¢size was favorable for longer creep lives. This was especially true at 982 °C.
6. The initial g¢size prior to testing was strongly influenced by bulk Re content, which likely decreased bulk diffusion. Decreasing negative values of lattice mismatch and lower g¢solvus temperatures also decreased initial g¢size, but these effects were not as potent as Re content.
7. TCP phase limits could not be directly ascertained because the alloy design primarily provided stable alloys. However, calculated deviations between actual lives and lives estimated by the 1093 °C

regression models indicated that TCP phase contents of up to ~2 vol% appeared tolerable under higher applied stresses where low creep lives of ~200 to 300 h were achieved. TCP phase contents of ~2 vol% were not tolerable at lower stress/longer life tests.

## References


1. R.C. Reed, The Superalloys: Fundamentals and Applications, Cambridge University Press, Cambridge, 2006.
2. A. Ma, D. Dye, R.C. Reed, Acta Mater. 56 (2008) 1657-1670.
3. Z. Zhu, H. Basoalto, N. Warnken, R.C. Reed, Acta Mater. 60 (2012) 4888-4900.
4. R.C. Reed, N. Matan, D.C. Cox, M.A. Rist, C.M.F. Rae, Acta Mater. 47/12 (1999) 3367-3381.
5. B.F. Dyson, M. McLean, Acta Metall. 31 (1983) 17-27.
6. M.V. Nathal, L.J. Ebert, Metall. Trans. 16A (1985) 1849-1862.
7. M.V. Nathal, L.J. Ebert, Metall. Trans. 16A (1985) 1863-1870.
8. T. Murakumo, T. Kobayashi, Y. Koizumi, H. Harada, Acta Mater. 52 (2004) 3737-3744.
9. P. Caron, C. Ramusat, F. Diologent, in: R.C. Reed, K.A. Green, P. Caron, T.P. Gabb, M.G. Fahrmann, E.S. Huron, S.A. Woodard (Eds.), Superalloys 2008, TMS, Warrendale, PA, 2008, pp. 159-167.
10. P. Caron, in: T.M. Pollock, R.D. Kissinger, R.R. Bowman, K.A. Green, M. McLean, S. Olson, J.J. Schirra (Eds.), Superalloys 2000, TMS, Warrendale, PA, 2000, pp. 737-746.
11. R.A. MacKay, M.V. Nathal, in: B.L. Bramfitt, R.C. Benn, C.R. Brinkman, G.F. Vander Voort (Eds.), MiCon 86: Optimization of Processing, Properties, and Service Performance Through Microstructural Control, ASTM STP 979, ASTM, Philadelphia, 1988, pp. 202-221. Also in NASA Technical Memorandum 88788, 1986.
12. M.V. Nathal, Metall. Trans. 18A (1987) 1961-1970.
13. R.A. MacKay, M.V. Nathal, D.D. Pearson, Metall. Trans. 21A (1990) 381-388.
14. M.V. Nathal, R.A. MacKay, R.G. Garlick, Mater. Sci. Eng. 75 (1985) 195-205.
15. M.V. Nathal, R.A. MacKay, R.G. Garlick, Scripta Metall. 22 (1988) 1421-1424.
16. T. Hino, T. Kobayashi, Y. Koizumi, H. Harada, T. Yamagata, in: T.M. Pollock, R.D. Kissinger, R.R. Bowman, K.A. Green, M. McLean, S. Olson, J.J. Schirra (Eds.), Superalloys 2000, TMS, Warrendale, PA, 2000, pp. 729-736.
17. F. Pyczak, B. Devrient, H. Mughrabi, in: K.A. Green, T.M. Pollock, H. Harada, T.E. Howson, R.C. Reed, J.J. Schirra, S. Walston (Eds.), Superalloys 2004, TMS, Warrendale, PA, 2004, pp. 827-836.
18. H. Harada, T. Yamagata, T. Yokokawa, K. Ohno, M. Yamazaki, in: Proc. 5th Int. Conf. on Creep and Fracture of Engineering Materials and Structures, Swansea, UK, 1993, pp. 255-264.
19. J.X. Zhang, T. Murakumo, Y. Koizumi, H. Harada, J. Mater. Sci. 38 (2003) 4883-4888.
20. N. Matan, D.C. Cox, C.M.F. Rae, R.C. Reed, Acta Mater. 47/7 (1999) 2031-2045.
21. T.P. Gabb, S.L. Draper, D.R. Hull, R.A. MacKay, M.V. Nathal, Mater. Sci. Eng. A118 (1989) 59-69.
22. Y. Koizumi, T. Kobayashi, T. Yokokawa, Z. Jianxin, M. Osawa, H. Harada, Y. Aoki, M. Arai, in: K.A. Green, T.M. Pollock, H. Harada, T.E. Howson, R.C. Reed, J.J. Schirra, S. Walston (Eds.), Superalloys 2004, TMS, Warrendale, PA, 2004, pp. 35-43.
23. P. Caron, T. Khan, Mater. Sci. Eng. 61(1983) 173-184.
24. R.A. MacKay, L. J. Ebert, in: M. Gell, C.S. Kortovich, R.H. Bricknell, W.B. Kent, J.F. Radavich (Eds.), Superalloys 1984, TMS, Warrendale, PA, 1984, pp. 135-144.
25. S. Neumeier, F. Pyczak, M. Göken, in: R.C. Reed, K.A. Green, P. Caron, T.P. Gabb, M.G. Fahrmann, E.S. Huron, S.A. Woodard (Eds.), Superalloys 2008, TMS, Warrendale, PA, 2008, pp. 109-119.
26. M. Simonetti, P. Caron, Mater. Sci. Eng. A254 (1998) 1-12.
27. J-B. Le Graverend, J. Cormier, S. Kruch, F. Gallerneau, J. Mendez, Metall. Mater. Trans. 2012; DOI:10.1007/s11661-012-1207-4

28. R.A. MacKay, L.J. Ebert, Metall. Trans. 16A (1985) 1969-1982.
29. R.C. Reed, T. Tao, N. Warnken, Acta Mater. 57 (2009) 5898-5913.
30. R.A. MacKay, T.P. Gabb, J.L. Smialek, M.V. Nathal, United States Patent 7,261,783 B1, Aug. 28, 2007.
31. R.A. MacKay, T.P. Gabb, J.L. Smialek, M. V. Nathal, NASA TM-2009-215819, National Aeronautics and Space Administration, Glenn Research Center, Oct. 2009.
32. R.A. MacKay, T.P. Gabb, J.L. Smialek, M.V. Nathal, JOM (2010) 48-54; DOI 10.1007/s11837-010-0011-0.
33. R.A. MacKay, T.P. Gabb, A. Garg, R.B. Rogers, M.V. Nathal, Mater. Char. 70 (2012) 83-100; http://dx.doi.org/10.1016/j.matchar.2012.05.001
34. R.A. MacKay, T.P. Gabb, A. Garg, R.B. Rogers, M.V. Nathal, NASA/TP-2012-217626, October 2012.
35. M.J. Donachie, S.J. Donachie, Superalloys: A Technical Guide, ASM International, Materials Park, OH, 2002, p. 30.
36. ASTM Designation: E139-11, in: Volume 3.01 Metals – Mechanical Testing: Elevated and Low-Temperature Tests: Metallography, 2012 Annual Book of ASTM Standards, West Conshohocken, PA, ASTM International, 2012, pp. 316-329.
37. Erratum in: Mater. Sci. Eng. 80 (1986) 101.
38. H. Harada, T. Yamagata, S. Nakazawa, K. Ohno, M. Yamazaki, in: Proc. High Temperature Materials for Power Engineering 1990, Liege, Belgium, 1990, pp. 1319-1328.
39. M. Pessah, P. Caron, T. Khan, in: S.D. Antolovich, R.W. Stusrud, R.A. MacKay, D.L. Anton, T. Khan, R.D. Kissinger, D.L. Klarstrom (Eds.), Superalloys 1992, TMS, Warrendale, PA, 1992, pp. 567-576.
40. A.F. Giamei, D.L. Anton, Metall. Trans. 16A (1985) 1997-2005.
41. G.R. Leverant, B.H. Kear, Metall. Trans. 1 (1970) 491-498.
42. T.M. Pollack, A.S. Argon, Acta Metall. Mater. 42/6 (1994) 1839-1874.
43. R.A. MacKay, M.V. Nathal, Acta Metall. Mater. 38/6 (1990) 993-1005.
44. M.V. Nathal, R.A. MacKay, Mater. Sci. Eng. 85 (1987) 127-138.
45. Y. Ro, Y. Koisumy, H. Harada, Mater. Sci. Eng. A223 (1997) 59-63.
46. J. Rüsing, N. Wanderka, U. Czubayko, V. Naundorf, D. Mukherji, J. Rösler, Scripta Mater. 46 (2002) 235-240.
47. S.C. Prasad, I.J. Rao, K.R. Rajagopal, Acta Mater. 53 (2005) 669-679.
48. A. Heckl, S. Neumeier, M. Göken, R.F. Singer, Mater. Sci. Eng. A 528 (2011) 3435-3444.

| REPORT DOCUMENTATION PAGE | Form Approved OMB No. 0704-0188 |
|---|---|



| 1. REPORT DATE *(DD-MM-YYYY)* | 2. REPORT TYPE | 3. DATES COVERED *(From - To)* |
|---|---|---|
| 01-04-2013 | Technical Memorandum | |

**4. TITLE AND SUBTITLE**
Effects of Microstructural Parameters on Creep of Nickel-Base Superalloy Single Crystals

**5a. CONTRACT NUMBER**

**5b. GRANT NUMBER**

**5c. PROGRAM ELEMENT NUMBER**

**6. AUTHOR(S)**
MacKay, Rebecca, A.; Gabb, Timothy, P.; Nathal, Michael, V.

**5d. PROJECT NUMBER**

**5e. TASK NUMBER**

**5f. WORK UNIT NUMBER**
WBS 473452.02.03.05.04.01.01

**7. PERFORMING ORGANIZATION NAME(S) AND ADDRESS(ES)**
National Aeronautics and Space Administration
John H. Glenn Research Center at Lewis Field
Cleveland, Ohio 44135-3191

**8. PERFORMING ORGANIZATION REPORT NUMBER**
E-18666

**9. SPONSORING/MONITORING AGENCY NAME(S) AND ADDRESS(ES)**
National Aeronautics and Space Administration
Washington, DC 20546-0001

**10. SPONSORING/MONITOR'S ACRONYM(S)**
NASA

**11. SPONSORING/MONITORING REPORT NUMBER**
NASA/TM-2013-217868

**12. DISTRIBUTION/AVAILABILITY STATEMENT**
Unclassified-Unlimited
Subject Category: 26
Available electronically at http://www.sti.nasa.gov
This publication is available from the NASA Center for AeroSpace Information, 443-757-5802

**13. SUPPLEMENTARY NOTES**

**14. ABSTRACT**
Microstructure-sensitive creep models have been developed for Ni-base superalloy single crystals. Creep rupture testing was conducted on fourteen single crystal alloys at two applied stress levels at each of two temperatures, 982 and 1093 °C. The variation in creep lives among the different alloys could be explained with regression models containing relatively few microstructural parameters. At 982 °C, γ - γ′ lattice mismatch, γ′ volume fraction, and initial γ′ size were statistically significant in explaining the creep rupture lives. At 1093 °C, only lattice mismatch and γ′ volume fraction were significant. These models could explain from 84 to 94 percent of the variation in creep lives, depending on test condition. Longer creep lives were associated with alloys having more negative lattice mismatch, lower γ′ volume fractions, and finer γ′ sizes. The γ - γ′ lattice mismatch exhibited the strongest influence of all the microstructural parameters at both temperatures. Although a majority of the alloys in this study were stable with respect to topologically close packed (TCP) phases, it appeared that up to ~2 vol% TCP phase did not affect the 1093 °C creep lives under applied stresses that produced lives of ~200 to 300 h. In contrast, TCP phase contents of ~2 vol% were detrimental at lower applied stresses where creep lives were longer. A regression model was also developed for the as-heat treated initial γ′ size; this model showed that γ′ solvus temperature, γ - γ′ lattice mismatch, and bulk Re content were all statistically significant.

**15. SUBJECT TERMS**
Superalloy; Creep; Single crystal; Microstructure; Nickel-base; Mechanical properties; Regression; Gamma prime; Lattice mismatch

| 16. SECURITY CLASSIFICATION OF: | | | 17. LIMITATION OF ABSTRACT | 18. NUMBER OF PAGES | 19a. NAME OF RESPONSIBLE PERSON |
|---|---|---|---|---|---|
| a. REPORT | b. ABSTRACT | c. THIS PAGE | | | STI Help Desk (email:help@sti.nasa.gov) |
| U | U | U | UU | 34 | 19b. TELEPHONE NUMBER *(include area code)* 443-757-5802 |